Adhesion of Colloids and Bacteria to Porous Media: A Critical Review

Runwei Li[1], Changfu Wei[2], Hefa Cheng[3] and Gang Chen[1,*]

[1]*Department of Civil and Environmental Engineering, FAMU-FSU College of Engineering, Florida State University, Tallahassee, FL 32310, USA*
[2]*State Key Laboratory Geomechanics and Geotechnical Engineering, Institute of Rock and Soil Mechanics, Chinese Academy of Sciences, Wuhan 430071, China*
[3]*College of Urban and Environmental Sciences, Peking University, Beijing 100871, China*

Abstract: Adhesion of colloids and bacteria to various surfaces is important for a variety of environmental phenomena including microbial biofouling and contamination prevention. Under saturated conditions, both colloids and bacteria have the opportunity to attach to porous medium surfaces. Under water unsaturated conditions or in the presence of the air-water interface, besides the porous medium surfaces, colloids and bacteria can also attach to the air-water interface, including the air-water-solid three-phase interface. The magnitudes of adhesion of colloids and bacteria are correlated to the interactions of the colloids and bacteria with the surfaces, which are a function of their surface physicochemical properties. In this review, adhesion theories are revisited and adhesion of colloids and bacteria to porous media and the air-water interface is discussed. The interaction forces are quantified using various theoretical models including the DLVO models and used to interpret related adhesion. The impact of surfactants on colloid and bacterial adhesion is also discussed. The review also includes the implementation of the adhesion theory in interpreting colloid and bacterial fate and transport in the subsurface soil.

Keywords: Adhesion, colloids, bacteria, porous media, air-water interface, interaction force

1. Introduction

Colloidal particles are small discrete solid particles present in natural porous media, which can be mobilized by means of hydrodynamic and other forces. They are composed of clay minerals with dimensions of micrometers and generally possess electric charges on their surfaces [1–3]. Colloids play important roles in

**Corresponding author:* gchen@eng.famu.fsu.edu

DOI: 10.7569/RAA.2019.097314

many natural and engineered systems. For instance, colloids present a potential health risk due to their propensity to associate with contaminants and facilitate their transport [3]. Bacteria are in the same size range as the colloids [4]. Similarly, bacteria pose health risk to human beings in the natural and engineered systems. Attachment of colloids and bacteria to various surfaces is important for a variety of environmental phenomena including microbial biofouling and contamination prevention. Though biological colloids (e.g., bacteria) and non-biological colloids (e.g., mineral colloids) differ in terms of surface characteristics, their attachment behaviors in the porous media share important similarities. The most fundamental similarity is that they are subjected to DLVO forces [5, 6]. Under saturated conditions, both colloids and bacteria have the opportunity to attach to porous media. However, under water unsaturated conditions or in the presence of the air-water interface, besides the porous media, colloids and bacteria can also attach to the air-water interface. Especially, at the air-water-solid three-phase interface, the attachment of colloids and bacteria is a complex phenomenon, which depends on the surface characteristics of the colloids, bacteria, porous media and the air-water interface and subsequent interactions [1, 2, 7].

There is a correlation between the magnitude of adhesion and the interactions of the colloids and bacteria with the surfaces, which are a function of their surface physicochemical properties [8]. Various theoretical models have been developed for the quantification of the interactions, which are then used to interpret the adhesion observations. In recent years, significant achievement has been made in investigation and development of adhesion theories of colloids and bacteria to the air-water interface. Accordingly, DLVO theory has been expanded to provide support for the adhesion observations [9–11]. It is necessary to identify the theory for adhesion of colloids and bacteria under various environmental conditions to rationalize the adhesion phenomena.

Adhesion of colloids and bacteria to porous media and the air-water interface controls their transport in the subsurface, which has received considerable attention either because they may contaminate drinking water supplies or because of their roles in in situ bioremediation [12, 13]. Since the adhesion is governed by the propensity to adhere to either the porous media or the air-water interface and is influenced by solution chemistry, the surface physicochemical properties of colloids, bacteria, porous media and the air-water interface as well as the transport conditions need to be characterized in order to quantify the adhesion kinetics and affinity of colloids and bacteria to these interfaces.

2. Adhesion Theory

2.1 Dupré Energy of Adhesion

Adhesion of colloids and bacteria to porous media or the air-water interface is attributed to their interactions with the surfaces or the interface, which is

DOI: 10.7569/RAA.2019.097314

determined by the surface free energies of colloids and bacteria. The solid surface free energy is often described in terms of the contact angle of a liquid on the given solid surface [14]. The relationship of contact angle θ, an indication of the balance of interfacial tensions between the liquid and solid, γ_{sl}, liquid and vapor, γ_{lv}, and solid and vapor, γ_{sv} can be described by the Young's equation [10] (Figure 1):

$$\gamma_{sl} = \gamma_{sv} - \gamma_{lv} cos\theta \tag{1}$$

Based on the Young equation, Owens-Wendt-Rabel-Kaelble (OWRK) developed a two-component model to describe the liquid-solid interfacial tension, including the dispersion (d) and polar (p) interactions between the phases [15]:

$$\gamma_{sl} = \gamma_{lv} + \gamma_{sv} - 2\left(\sqrt{\gamma_{lv}^{d}\gamma_{sv}^{d}} + \sqrt{\gamma_{lv}^{p}\gamma_{sv}^{p}}\right) \tag{2}$$

where γ_{lv}^{d}, γ_{sv}^{d}, γ_{lv}^{p}, and γ_{sv}^{p} are the dispersion and polar components of the interfacial tension between the liquid and vapor and between solid and vapor. After combining the above equations, the OWRK equation is obtained [16]:

$$\gamma_{lv}(1+cos\theta) = 2\left(\sqrt{\gamma_{lv}^{d}\gamma_{sv}^{d}} + \sqrt{\gamma_{lv}^{p}\gamma_{sv}^{p}}\right) \tag{3}$$

The OWRK equation is used to find two unknowns, γ_{sv}^{d} and γ_{sv}^{p}, and thus contact angle measurements with at least two liquids with known γ_{lv}^{d} and γ_{lv}^{p} are needed. One liquid should be dominantly polar (e.g., water or glycerol) and the other liquid should be dispersive (e.g., diiodomethane) [10]. With the determined γ_{sv}^{d} and γ_{sv}^{p}, the total interfacial free energy of the solid-vapor interface, γ_{sv} can be calculated as $\gamma_{sv} = \gamma_{sv}^{d} + \gamma_{sv}^{p}$. The OWRK method is one of the commonly used approaches to determine the surface free energy of solids using contact angle measurements [17, 18].

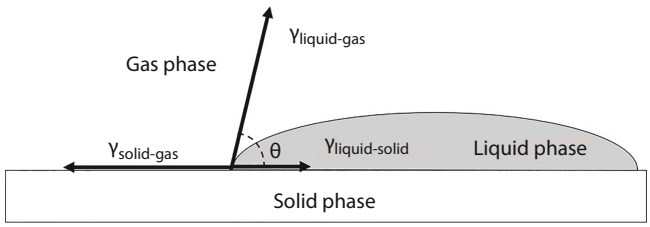

Figure 1 The Relationship of Contact Angle and Interfacial Tensions by the Young Equation. A liquid drop forms a contact angle θ on a solid surface, which is an indication of the balance of interfacial tensions between the liquid and solid, $\gamma_{liquid\text{-}solid}$, liquid and gas, $\gamma_{liquid\text{-}gas}$ and solid and gas $\gamma_{solid\text{-}gas}$.

DOI: 10.7569/RAA.2019.097314

In the above two-component model, the interfacial tension depends on whether the polar and dispersion components of the surface tension are involved in the interactions with the corresponding components of the bordering phase. Although it was originally developed to interpret wettability, the two-component model has contributed much more beyond that. The two-component model has been extended to a three-component model, in which the polar component has been further split into a fraction for dipole-dipole interactions, γ^p and a hydrogen bonding fraction, γ^h [19]:

$$\gamma_{sl} = \gamma_{lv} + \gamma_{sv} - 2\left(\sqrt{\gamma_{lv}^d \gamma_{sv}^d} + \sqrt{\gamma_{lv}^p \gamma_{sv}^p} + \sqrt{\gamma_{lv}^h \gamma_{sv}^h}\right) \tag{4}$$

where γ_{lv}^p, γ_{sv}^p, γ_{lv}^h and γ_{sv}^h are the dipole-dipole component and hydrogen bonding component of the interfacial tension between the liquid and vapor and between the solid and vapor. It should be noted that hydrogen bonds have greater bonding energy than the dispersion and dipole-dipole interactions [19]. The wettability of a solid by water depends to a great extent on the ability of the solid to form hydrogen bonds [19]. Correspondingly, the OWRK equation is expressed as:

$$\gamma_{lv}(1 + cos\theta) = 2\left(\sqrt{\gamma_{lv}^d \gamma_{sv}^d} + \sqrt{\gamma_{lv}^p \gamma_{sv}^p} + \sqrt{\gamma_{lv}^h \gamma_{sv}^h}\right) \tag{5}$$

Based on the acid-base concept model, van Oss, Chaudhury and Good further split the polar component into an electron-acceptor parameter, γ^+ and an electron-donor parameter, γ^-. They further advanced the approach by replacing the dispersion and dipole-dipole interactions with the Lifshitz-van der Waals component [19]:

$$\gamma_{sl} = \gamma_{lv} + \gamma_{sv} - 2\left(\sqrt{\gamma_{lv}^{LW} \gamma_{sv}^{LW}} + \sqrt{\gamma_{lv}^+ \gamma_{sv}^-} + \sqrt{\gamma_{sv}^+ \gamma_{lv}^-}\right) \tag{6}$$

where γ^{LW} is the Lifshitz-van der Waals component of surface tension, consisting of dispersion, polar, and induced polar interactions, and γ^+ and γ^- are the electron-acceptor and electron-donor parameters of the acid-base component of surface tension. On the other hand, Wu proposed a reciprocal or harmonic mean as opposed to the geometric mean, claiming the geometric mean approach was not applicable to polar-polar system [20–22]:

$$\gamma_{sl} = \gamma_{lv} + \gamma_{sv} - 4\left[\frac{\gamma_{sv}^d \gamma_{lv}^d}{\gamma_{sv}^d + \gamma_{lv}^d} + \frac{\gamma_{sv}^p \gamma_{lv}^p}{\gamma_{sv}^p + \gamma_{lv}^p}\right] \tag{7}$$

DOI: 10.7569/RAA.2019.097314

The van Oss-Chaudhury-Good equation is finally obtained [10]:

$$\gamma_{lv}(1+cos\theta)=2\left(\sqrt{\gamma_{lv}^{LW}\gamma_{sv}^{LW}}+\sqrt{\gamma_{lv}^{+}\gamma_{sv}^{-}}+\sqrt{\gamma_{sv}^{+}\gamma_{lv}^{-}}\right) \tag{8}$$

Since the van Oss-Chaudhury-Good method has three unknows, γ_{sv}^{LW}, γ_{sv}^{+} and γ_{sv}^{-}, three contact angle measurements with three liquids are required: one dispersive liquid (e.g., diiodomethane), and two polar liquids (e.g., water and glycerol). This approach has the potential to provide more in-depth insight into the surface properties. Accordingly, when combining with the OWRK equation, the Wu equation can be extended as [15, 23]:

$$\gamma_{lv}(1+cos\theta)=4\left[\frac{\gamma_{sv}^{d}\gamma_{lv}^{d}}{\gamma_{sv}^{d}+\gamma_{lv}^{d}}+\frac{\gamma_{sv}^{p}\gamma_{lv}^{p}}{\gamma_{sv}^{p}+\gamma_{lv}^{p}}\right] \tag{9}$$

Like the OWRK method, two liquids: one polar and one dispersive, are needed to determine the surface free energy. In practice, the OWRK method is generally more accurate than the Wu method.

2.2 *Lifshitz-van der Waals Forces*

Lifshitz-van der Waals forces, as non-covalent forces, arise from the fluctuations in the electric dipole moments of molecules. In 1893, a thermodynamic theory was developed by Johannes D. van der Waals to include three force contributions of different origins [24]:

$$w(r)=\frac{C_{ind}+C_{orient}+C_{disp}}{r^{6}}=-\frac{C_{vdW}}{r^{6}} \tag{10}$$

where $w(r)$ is the van der Waals force, which is a function of r, the distance between the molecules, C_{ind}, C_{orient}, and C_{disp} are the force coefficients due to induction, orientation and dispersion, respectively. All the three force contributions are proportional to $1/r^6$ and the total van der Waals force coefficient, C_{vdW} is given by [24]:

$$C_{vdW}=-\left[\frac{\mu_1^2\mu_2^2}{3(4\pi\varepsilon_0\varepsilon)^2k_BT}+\frac{\mu_1^2\alpha_2+\mu_2^2\alpha_1}{(4\pi\varepsilon_0\varepsilon)^2}\right]_{\nu=0}+\left[\frac{3\alpha_2\alpha_1}{2(4\pi\varepsilon_0\varepsilon)^2}\frac{h\nu_1h\nu_2}{\nu_1+\nu_2}\right]_{\nu>0} \tag{11}$$

where α_1 and α_2 are the electronic polarizabilities of the molecules, μ_1 and μ_2 are the dipole moments, ε_0 is the vacuum permittivity, k_B is the Boltzmann constant,

DOI: 10.7569/RAA.2019.097314

T is the absolute temperature, hv_1 and hv_2 are the first ionization potentials of the molecules, v_1 and v_2 are the ionized frequencies, and h is the Planck constant. The first term on the right side of the equation (i.e., v=0) is attributed to the Keesom and Debye contributions and is only valid for interactions between polar molecules. The second term (i.e., v>0) is attributed to the dispersion or London contribution and is valid for all molecules.

Keesom force is initiated by permanent dipole-permanent dipole interactions between polar molecules; Debye force is initiated by permanent dipole-induced dipole interactions between a polar molecule and a temporarily polarized non-polar molecule that is induced by the distortion of charge cloud and subsequent charge fluctuations in the electron distribution; and London force is initiated by instantaneous induced dipole-induced dipole interactions between temporarily polarized non-polar molecules caused by the movement of electrons (Figure 2). It should be noted that Keesom force and Debye force are much stronger than London force for molecules of equivalent size. For all of these three forces, the strength is related to the number of electrons and hence to the size of the molecules.

The van der Waals force is the sum of Keesom, Debye and London forces, and is responsible for aggregation and adhesion. The Keesom, Debye and London forces can be quantified by the enthalpy associated with the phase transition from liquid to gas, ΔH_{vap} [25]. Thus, gas-phase measurements and computational methods are commonly combined to quantify the van der Waals force [26]. However, solvent effects such as solvent cohesion or solvophobic effects complicate the quantification of van der Waals force in the solution, which is described by the Hildebrand solubility parameter, δ_H [27]:

$$\delta_H = \sqrt{\frac{\Delta H_{vap} - RT}{V_m}} \tag{12}$$

where R is the gas constant and V_m is the molar volume of the particular solvent at temperature T.

2.3 *Lewis Acid/Base Forces*

Water-mediated Lewis acid/base interactions are initiated by the different water density in the solvation or hydration layer [28]. Near the particle surface, the distribution of water molecules is impacted by the electron-donor (i.e., hydrogen-acceptor) and electron-acceptor (i.e., hydrogen-donor) potentials of the particle surfaces. For particles having both γ^- and γ^+ values greater or smaller than those of water, the hydrogen-donor and hydrogen-acceptor parameters of the acid-base component of surface tension are nearly balanced relative to that of water within the very thin water layer. Thus, the solvation layer has a density

DOI: 10.7569/RAA.2019.097314

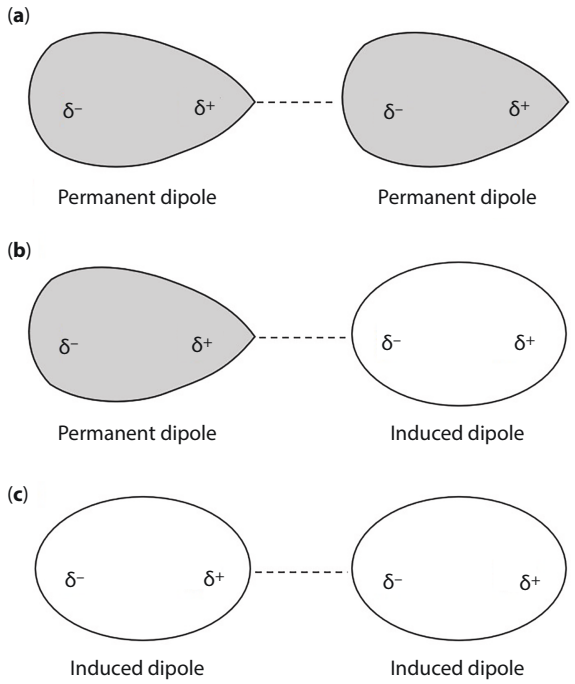

Figure 2 Keesom (a), Debye (b) and London (c) contributions to van der Waals Forces: (a) Keesom force is initiated by permanent dipole-permanent dipole interactions between polar molecules; (b) Debye force is initiated by permanent dipole-induced dipole interactions between a polar molecule and a temporarily polarized non-polar molecule that is induced by the distortion of charge cloud and subsequent charge fluctuations in the electron distribution; and (c) London force is initiated by instantaneously induced dipole-induced dipole interactions between temporarily polarized non-polar molecules caused by the movement of electrons.

less than that of the bulk liquid [29]. Under these conditions, a negative surface excess of water occurs, leading to the surfaces being pushed together by the bulk liquid. The interactions between the surfaces are thus attractive with the strength proportional to the absolute value of the negative surface excess. In contrast, for particles having unmatched γ^- and γ^+ values (i.e., one is greater and the other is smaller than those of water), more water molecules are needed to balance the hydrogen-donor and hydrogen-acceptor potentials. The solvation layer thus has a greater density than that of the bulk liquid, resulting in a positive surface excess of water, which separates the surfaces [30]. Correspondingly, the interactions between the surfaces are repulsive and the strength is proportional to the absolute value of the positive surface excess.

DOI: 10.7569/RAA.2019.097314

As discussed above, three contact angle measurements with three liquids are required to quantify γ_{sv}^{LW}, γ_{sv}^{+} and γ_{sv}^{-}: one dispersive liquid (e.g., diiodomethane), and two polar liquids (e.g., water and glycerol). With the introduction of the Lewis acid/base concept, the surface tension of the measuring liquids and the surface free energy of the solid surfaces can be expressed as [10]:

$$\gamma = \gamma^{LW} + 2\sqrt{\gamma^{+}\gamma^{-}} \tag{13}$$

Subsequently, the van Oss-Chaudhury-Good equation becomes [10]:

$$(1+cos\theta)\left(\gamma_{lv}^{LW} + 2\sqrt{\gamma_{lv}^{-}\gamma_{lv}^{+}}\right) = 2\left(\sqrt{\gamma_{sv}^{LW}\gamma_{lv}^{LW}} + \sqrt{\gamma_{sv}^{+}\gamma_{lv}^{-}} + \sqrt{\gamma_{sv}^{-}\gamma_{lv}^{+}}\right) \tag{14}$$

Polar liquids with both the largest and smallest polar components should be included in the measurement [31, 32]. As a polar liquid, water, whose surface thermodynamic properties are well known, is a frequently measuring liquid paired with two other liquids. Diiodomethane, on the other hand, is an ideal dispersive liquid as it has a relatively high surface tension and forms easily measurable contact angles with many solids [33].

2.4 Hydration Forces

Hydration forces are short range interactions, which become important when the separation distances are in the range of nanometers [34]. As additional contributions to the disjoining pressure of Lewis acid/base forces, they are usually ignored when the separation distances are greater than 1 to 2 nm [35]. The hydration forces, $F(D)$ as a function of separation distance D are typically approximated from the Lifshitz-van der Waals forces [35]:

$$F(D) = \pi R^2 \Pi_{vdW}(D) \tag{15}$$

where $\Pi_{vdW}(D)$ is the Lifshitz-van der Waals force and R is the size of the molecules or particles. By ignoring retardation effects,

$$\Pi_{vdW}(D) = -\frac{A}{6\pi D^3} \tag{16}$$

where A is the Hamaker constant.

DOI: 10.7569/RAA.2019.097314

2.5 *Electrical Double Layer Forces*

Electrical double layer forces are interactions between charged molecules or particles. Owing to the difficulty of the direct measurement, expression of the electrical double layer interactions, Π_{el} is limited to indirect quantification [36]:

$$\Pi_{el} = k_B T \sum_i \left(C_i(z) - C_{i,\infty}\right) - \frac{\varepsilon\varepsilon_0}{2}\left(\frac{d\psi}{dz}\right)^2 \tag{17}$$

where $C_i(z)$ is the ion concentration of species i at distance z, $C_{i,\infty}$ is the bulk concentration of the corresponding ion, ε and ε_0 are the relative dielectric permittivity of water and permittivity of vacuum, respectively, and ψ is the surface potential, which can be calculated by [37]:

$$\psi = \xi\left(1 + \frac{z}{R}\right)\exp(\kappa z) \tag{18}$$

where ζ is the zeta potential, R is the size of colloids or bacteria, k is the Boltzmann constant, and $1/\kappa$ is the Debye-Hückel length, which is also an estimation of the effective thickness of the electrical double layer.

In the electrical double layer force equation, the first term is the contribution due to osmotic repulsion caused by local variation of the ion concentration of all ionic species in the system and the second one is due to direct electrostatic interaction, which can be attractive or repulsive depending on the surface charges [38]. The solution of the equation depends on the unknown functions $C_i(z)$ and $\psi(z)$, i.e., the concentration profiles of all ionic species and electrostatic potential in the electrolyte at an arbitrary position. The concentration of ions follows the Boltzmann distribution [39]:

$$C_i(z) = C_{i,\infty} e^{\left(-\frac{Z_i e\psi(z)}{k_B T}\right)} \tag{19}$$

where e represents the electron charge, z_i is the valency of corresponding ion, k_B is the Boltzmann constant, and T is the absolute temperature. The potential distribution $\psi(z)$ can be numerically obtained by solving the Poisson–Boltzmann equation using the standard Runge–Kutta algorithm [40]:

$$\frac{d^2}{dz^2}\psi(z) = -\frac{e}{\varepsilon\varepsilon_0}\sum_i Z_i C_{i\infty} \exp\left(-\frac{Z_i e\psi(z)}{k_B T}\right) \tag{20}$$

DOI: 10.7569/RAA.2019.097314

Above equations further indicate that electrical double layer forces depend directly on the ion distribution in the diffuse part of the double layer.

The diffusion of ions can be determined from electrical conductivities or diffusion experiments, which is related to the ionic mobility μ by the Nernst-Einstein equation [41]:

$$D = \frac{\mu RT}{zF} \tag{21}$$

where D is the diffusion coefficient, R is the universal gas constant, T is the absolute temperature, z is the ionic valence, and F is the Faraday constant. The equivalent conductivity of an ion, Λ, is related to its mobility by $\Lambda = F\,\mu$ and is quantified by [41]:

$$\Lambda = \frac{K}{C} \tag{22}$$

where K is the specific conductivity of the bulk solution and C is the concentration of the solution.

2.6 *Quantitative Structure–Activity Relationship (QSAR) Analysis*

Interactions can also be quantified based on the quantitative structure–activity relationship (QSAR) analysis, a practical approach to quantitatively correlate the chemical structures of the functional groups on the surfaces with the molecular interactions [42]. A wide variety of molecular descriptors, including molecular weight, molar volume, numbers of the specific types of atoms or bonds, molecular connectivity index, and complex 3-D geometrical descriptors are used in the interaction quantification by QSAR analysis [43]. Singly-descriptor-based and multi-descriptor-based predictive statistical QSAR models have been developed with the chemical structure information numerically encoded in the form of descriptors [44]. Currently, there is a constant effort in developing more efficient QSAR techniques to accurately quantify molecular interactions. A typical example is the use of 3-D geometrical descriptors, which more accurately estimate the intermolecular interactions by taking the geometric structure of the molecule into consideration.

2.7 *Capillary Forces*

In the presence of the air-water interface, colloids and bacteria are also subject to the capillary forces. Capillarity is the result of adhesion of water molecules to

DOI: 10.7569/RAA.2019.097314

a solid surface by surface tension [45]. The most commonly observed case is a narrow glass tube inserted in water with openings at both ends, in which water is drawn upward. The narrower the tube is, the greater the rise of water is. The rise of water is also a function of water surface tension and ratio of adhesion to cohesion [46]. Capillary forces lead to the formation of a meniscus for the liquid that is confined in a tube. For a meniscus with principal radii of curvature R_1 and R_2, the pressure difference across the meniscus is described by the Laplace equation [46] (Figure 3):

$$P_{atm} - P_{liquid} = \gamma\left(\frac{1}{R_1} + \frac{1}{R_2}\right) \tag{23}$$

where P_{atm} is the atmospheric pressure, P_{liquid} is the Laplace pressure in the liquid, and γ is the surface tension of the liquid. For meniscus with a small radius, the gravitational effects are negligible.

The shape of the meniscus forms a section of a cylinder with a radius governed by the contact angle of the rinsing liquid on the sidewall, θ. Under these conditions, $R_1 = R_2 = R$ [46]:

$$R = \frac{2\gamma cos\theta}{\rho gh} \tag{24}$$

where h is the height of the meniscus and ρ is the density of the liquid. For 0^o contact angle, the above equation becomes:

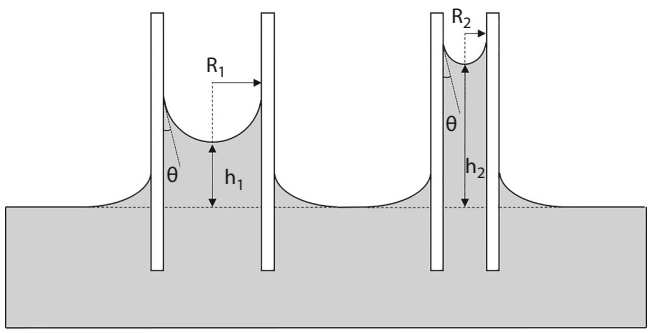

Figure 3 Capillary Force by Laplace Equation. Menisci with principal radii of curvature R_1 and R_2 are shown in this figure with water rise of h_1 and h_2. For meniscus with a small radius like R_2, the gravitational effects are negligible.

DOI: 10.7569/RAA.2019.097314

$$R = \frac{2\gamma}{\rho g h} \tag{25}$$

When a narrow glass tube is inserted into mercury, because the contact angle is > 90°, the mercury level is not raised but depressed below the level of the surrounding liquid.

Equilibrium surface tension can be measured based on capillary rise using the wicking method following the Young–Laplace equation [47]. The applied pressure, ΔP, across a curved interface with a radius of curvature, R_c has the following relationship with interfacial tension, γ,

$$\Delta P = \frac{2\gamma}{R_c} \tag{26}$$

R_c is the radius of curvature that equals the radius of the circular arc. The accuracy and reproducibility of the measurement system can be checked by making an equilibrium surface tension measurement on a clean air-water interface.

3. Adhesion of Colloids and Bacteria at Interfaces

3.1 Adhesion at the Liquid-Solid Interface

Under water saturated conditions, colloids and bacteria attach to the porous media as a result of the net force between colloids or bacteria and the porous media, which is strongly dependent on the separation distance [48, 49]. For most cases, the colloids and bacteria as well as the porous media are negatively charged. Subsequently, colloids and bacteria have repulsive electrical double layer forces with the porous media. In addition, the electrical double layer forces are greatly affected by the solution chemistry in terms of solution ionic strength and pH. Subsequently, change of solution ionic strength and pH impacts the adhesion of colloids and bacteria to the porous media [50, 51]. Because of the nature of the forces, colloids and bacteria have attractive Lifshitz–van der Waals forces and Lewis acid/base forces. With the decrease of the separation distance, electrical double layer forces and Lifshitz–van der Waals forces drop, while Lewis acid/base forces increase (Figure 4). It should be noted that the decrease of electrical double layer forces is more pronounced than those of Lifshitz-van der Waals forces and Lewis acid/base forces [52, 53]. At the equilibrium distance where the adhesion of colloids and bacteria to the porous media occurs, the attractive Lewis acid/base forces dominate over repulsive electrical double layer forces, resulting in colloid and bacterial adhesion [10, 54–56].

DOI: 10.7569/RAA.2019.097314

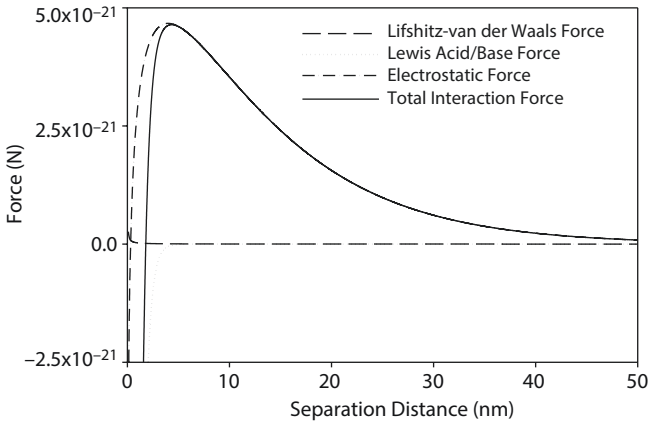

Figure 4 Interaction Force as a Function of Separation Distance. After overcoming the repulsive force barrier, electrical double layer forces and Lifshitz–van der Waals forces decrease, while Lewis acid/base forces increase with the decrease of the separation distance.

In the solution, when colloids or bacteria get close to the porous media, they first suffer from the long-range repulsive electrical double layer forces. Therefore, reduction of the repulsive electrical double layer forces in the system would be favorable for colloid and bacterial adhesion. The lowing of the repulsive electrical double layer forces can be achieved by increase of the solution ionic strength, which compresses the double layers of both the colloids or bacteria and the porous media [57]. Solution pH also impacts the repulsive electrical double layer forces through the adsorption of OH^- and H^+ on the colloid, bacterial and porous medium surfaces [58]. At high pH, colloid, bacteria and porous media are more negatively charged owing to the predominant existence of OH^-, resulting in increased repulsive electrical double layer forces. At low pH, colloid, bacteria and porous media are more positively charged owing to the predominant existence of H^+, resulting in increased oppositely charged repulsive electrical double layer forces. At intermediate pH, the charges on colloids, bacteria and porous media decrease, leading to decreased repulsive electrical double layer forces and possibly adhesion [2, 59, 60].

Adhesion of colloids and bacteria to porous media leads to variations in system's Gibbs free energy due to the change of the surfaces (i.e., colloid-liquid, bacterial-liquid and porous medium-liquid interfaces become colloid-porous medium or bacterial-porous medium interfaces by adhesion), which can be related to interfacial tensions [10, 61]:

$$\Delta G_{adh} = (\gamma_{ps} - \gamma_{pl} - \gamma_{sl})A \tag{27}$$

where ΔG_{adh} is system's Gibbs free energy change due to adhesion, γ_{ps}, γ_{pl} and γ_{sl} are colloid- or bacterial (p)-porous medium (s), colloid- or bacterial (p)-liquid (l), and

DOI: 10.7569/RAA.2019.097314

porous medium (*s*)-liquid (*l*) interfacial tensions, respectively, and A is the adhesion area. Change in solution chemistry such as the presence of surfactant (which will be discussed in the later sections) leads to variations of γ_{ps}, γ_{pl} and γ_{sl}, which eventually results in different adhesion (Figure 5).

The interfacial tension can be calculated according to equations described before. The adhesion is favored if ΔG_{adh} is negative and unfavored if ΔG_{adh} is positive. Interfacial tensions γ_{pl} and γ_{sl} are also correlated with ΔG_{plp} and ΔG_{sls}, the interaction free energy between colloids or bacteria or between the porous medium when immersed in the liquid [10]:

$$\Delta G_{plp} = -2\gamma_{pl} \tag{28}$$

$$\Delta G_{sls} = -2\gamma_{sl} \tag{29}$$

From the surface thermodynamic perspective, colloids, bacteria or porous media are hydrophilic with respect to the liquid "*l*" if ΔG_{plp} *or* $\Delta G_{sls} > 0$ and hydrophobic if ΔG_{plp} *or* $\Delta G_{sls} < 0$. The hydrophilicity or hydrophobicity increases with the increase of absolute value of ΔG_{plp} or ΔG_{sls}.

When colloids and bacteria are in solution, they are also subjected to hydrodynamic forces in addition to the DLVO forces. It should be noted that the hydrodynamic forces are at a 90° angle to the DLVO forces that include electrical double layer forces, Lifshitz–van der Waals forces and Lewis acid/base forces [62]. Adhesion of colloids and bacteria to porous media is possible if the torque of the net effect of attractive Lifshitz–van der Waals and Lewis acid/base forces and

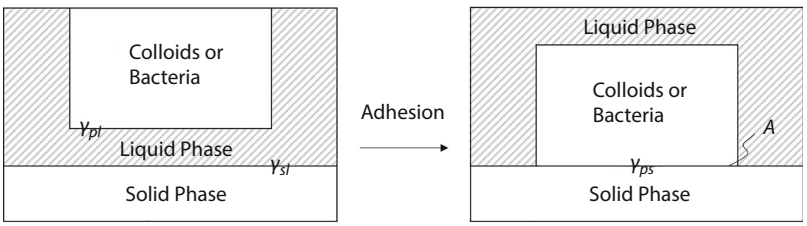

Figure 5 Gibbs Free Energy Change after Adhesion. Adhesion of colloids and bacteria to porous media leads to variations in system's Gibbs free energy due to the change of the surfaces (i.e., colloid-liquid, bacterial-liquid and porous medium-liquid interfaces become colloid-porous medium or bacterial-porous medium interfaces by adhesion. ΔG_{adh} is system's Gibbs free energy change due to adhesion, γ_{ps}, γ_{pl} and γ_{sl} are colloid- or bacterial (p)-porous medium (*s*), colloid- or bacterial (*p*)-liquid (*l*), and porous medium (*s*)-liquid (*l*) interfacial tensions, respectively, and A is the adhesion area.

DOI: 10.7569/RAA.2019.097314

repulsive electrical double layer forces balances the torque of the hydrodynamic forces at the equilibrium distance where colloids or bacteria adhere to porous media [6]. On the contrary, if the torque of the hydrodynamic forces cannot be balanced by the net effect of attractive Lifshitz–van der Waals and Lewis acid/base forces and repulsive electrical double layer forces, adhesion cannot occur and colloids and bacteria move along with the flow of the solution.

3.2 Adhesion at the Air-Water Interface

The air-water interface is responsible for capillary forces. Besides, the air-water interface also has direct interactions with colloids and bacteria, making it possible for them to attach [63, 64]. Adhesion of colloids and bacteria to the air-water interface is determined by their mutual interactions, which can be estimated by the thermodynamic quantification in terms of Gibbs free energy to interpret the adhesion. Similarly to adhesion of colloids and bacteria to the porous media, the interactions between colloids and bacteria begin with repulsive electrical double layer forces since colloids, bacteria and the air-water interface are negatively charged [1, 2, 7, 65]. The repulsive electrical double layer forces are separation distance dependent, which decrease significantly with the increase of the separation distance. When colloids and bacteria are in the nanometer range to the air-water interface, hydrophobic interactions lead to the adhesion of colloids and bacteria to the air-water interface [6, 66]. When colloids and bacteria are exposed to both the gas phase and the liquid phase, capillary forces are also involved in the adhesion, which are usually the dominant forces over others. Moving air-water interface can also mobilize the attached colloids and bacteria. Thermodynamic calculations indicate that the air-water interface is more favorable for colloids and bacteria to attach as compared with the suspension phase, except for hydrophilic colloids in the nanometer size range [67].

3.2.1 Water Structure and Hydrogen Bonding

Water structure must be clearly understood for an accurate quantification of the interactions between colloids or bacteria and the air-water interface. In water, water molecules are attracted to each other by forming hydrogen bonds, which are initiated by attractive interactions between the hydrogen atoms and the oxygen atoms [68]. In such systems, each water molecule has four hydrogen bonding arms, with each arm having the capacity to form a single hydrogen bond and adopt a continuum of orientations [69]. The oxygen atom of a water molecule is located at the center of the symmetric tetrahedral configuration with the inter-arm angle equal to 109^{o} (Figure 6). For water molecules to form hydrogen bonds with each other, the tips of two hydrogen atoms are positioned towards one oxygen atom with the length of the hydrogen bonding-arms equal to the hydrogen bond length, which is assumed to be independent of whether the water molecules are in the bulk or at the surface [70].

DOI: 10.7569/RAA.2019.097314

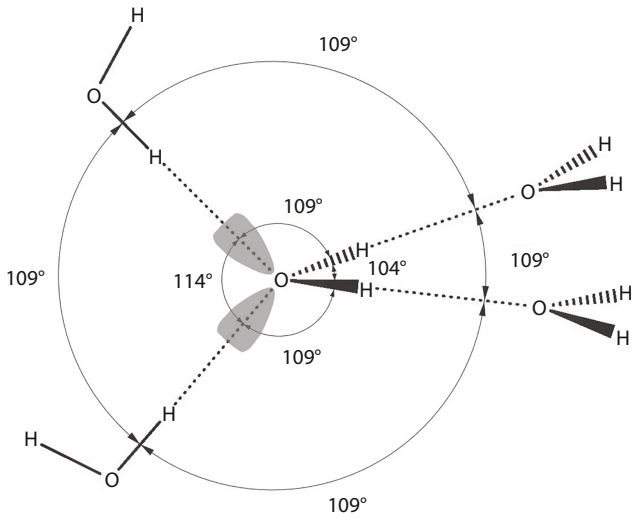

Figure 6 Symmetric Tetrahedral Configuration of Water Molecule. The oxygen atom of a water molecule is located at the center of the symmetric tetrahedral configuration with the inter-arm angle equal to 109°.

At the air-water interface, water molecules are subject to interactions in three directions instead of four (i.e., no interactions in the direction of the air). The thus unbalanced interactions lead to the establishment of stronger hydrogen bonds at the water surface, resulting in the formation of the surface tension, which makes the surface area as small as possible to minimize the required work [71]. Hydrogen-bonding energy, the energy of the interactions between the hydrogen and oxygen atoms, is commonly used to describe the hydrogen bond strength, which has a typical enthalpy of 21 kJ/mol or 5.0 kcal/mol in vapor [72]. Similarly to the air-water interface, when two different phases (i.e., gas/liquid, liquid/liquid, gas/solid or liquid/solid) are in contact with each other, interfaces are formed. At the interfaces, the molecules experience imbalanced forces, leading to an accumulation of free energy. The excess free energy is usually quantified by the measurement of the energy to area ratio or the energy required to increase the unit area of the interface [73, 74]. Another way to describe the above phenomena is through interfacial tension. The interfacial tension or the excess free energy at the interface, which is also called adhesion force, is attributed to the interactions between different molecules [75, 76].

Hydrogen bonds can also be formed between water molecules and functional groups including hydroxyl, carbonyl, and carboxyl groups, etc., which commonly exist on colloid and bacterial surfaces [77–79]. The hydroxyl group, denoted by -OH, consists of a hydrogen atom covalently bonded to an oxygen atom and is

DOI: 10.7569/RAA.2019.097314

present in alcohols and carboxylic acid molecules. The carbonyl group contains a covalent C=O double bond and is present in aldehydes, ketones, esters, anhydrides, and carboxylic acids. The carboxyl group is the monovalent group of -COOH, consisting of a carbonyl group bound to a hydroxyl group and is the main functional group in organic acids (i.e., carboxylic acids) [80]. Carboxylic acids also form hydrogen bonds with each other (Figure 7). Unique to carboxylic acids, hydrogen bonding can occur between two molecules to produce a dimer [81, 82]. The presence of dimers increases the strength of the van der Waals dispersion forces. As illustrated in Figure 8, formation of hydrogen bonds occurs between the C=O bonds of carboxylic group and the O-H bonds of water. Although the hydrogen bonds are relatively weak compared to the covalent bonds within the water molecule itself, the formed hydrogen bonds lead to changes in physical properties [83]. For instance, hydrogen bonds result in relatively higher boiling point because more heat energy is required to break the hydrogen bonds. Similarly, the hydrogen bonds also provide water a higher cohesiveness and, consequently, a greater surface tension.

The polarity of the H–O bonds plays the key role for the formation of the hydrogen bonds as the hydrogen bonding arises from the attraction between electron-deficient hydrogen atoms (i.e., δ^+) and lone pairs of electrons on oxygen atoms (i.e., δ^-), which are sufficiently electronegative to withdraw electron density in the H–O bonds away from the hydrogen atoms, resulting in the hydrogen

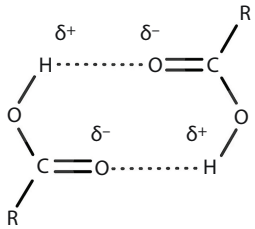

Figure 7 Hydrogen Bond Formation between Carboxylic Acids. Carboxylic acids consist of -COOH, i.e., a carbonyl group bound to a hydroxyl group. Carboxylic acids thus form hydrogen bonds with each other.

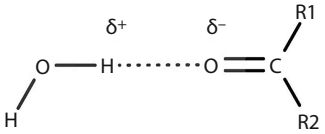

Figure 8 Hydrogen Bond Formation between Carboxylic Acids and Water. The C=O bonds of carboxylic group and the O-H bonds of water form hydrogen bonds.

DOI: 10.7569/RAA.2019.097314

atoms being attracted to the lone pairs (Figure 8) [84, 85]. Carboxylic acids are weak acids. Subsequently, deprotonation due to the strong stabilizing resonance formed by two oxygen atoms, releasing H^+ cations and $RCOO^-$ anions in neutral aqueous solvents such as water [86]. $[H^+]_0$ deviates from the bulk concentration $[H^+]_\infty$, which is fixed by the pH, i.e., pH = $-\log[H+]_\infty$. $[H^+]_0$ is assumed to follow the Boltzmann distribution [87]:

$$[H^+]_0 = [H^+]_\infty e^{-e\psi_0/k_BT} \tag{30}$$

where e is the charge of the electron, ψ_0 is the potential measured at the surface, k_B is the Boltzmann constant, and T is the absolute temperature.

Hydrogen-bonds are also used to define acidity and basicity. Hydrogen-bond donors (D-H) are acids (i.e., A-H) with dissociation constant $K_a = K^0_{AH}$ and hydrogen-bond acceptors (:A) are bases (i.e., B or carboxyl functional groups) with dissociation constant $K_a = K^0_{BH^+}$ according to [88, 89]:

$$AH(H_2O) + H_2O \overset{K^0_{AH}}{\Leftrightarrow} H_3O^+(H_2O) + A^-(H_2O) \tag{31}$$

$$BH^+(H_2O) + H_2O \overset{K^0_{BH^+}}{\Leftrightarrow} H_3O^+(H_2O) + B(H_2O) \tag{32}$$

Hydrogen bonds are symbolized as D-H···:A. When hydrogen bonds are formed, the difference in the acidity constants, ΔpK_a, is calculated as:

$$\Delta pK_a(D - H \cdots: A) = pK_a(D - H) - pK_a(A - H^+) \tag{33}$$

ΔpK_a is negative or positive depending on whether or not the $D{:}^- \cdots H - A^+$ proton transfer occurs. The strength of hydrogen bonds is determined by $|\Delta pK_a|$. The smaller the $|\Delta pK_a|$ is, the shorter and stronger the hydrogen bond is. Hydrogen bonds between carboxyl functional groups and between carboxyl functional groups and water should have a $|\Delta pK_a|$ value of ~16 – 18 based on the fundamental force of dipole-dipole interactions [88, 89]. Accordingly, the hydrogen-bonds strength is ~ 4 – 17 kJ/mole.

3.2.2 Air-Water Interface Charges

The charge at the air-water interface is negative as measured by electrophoresis on air bubbles, which arises from an excess of OH^- as a result of the preferential orientation of water molecules at the air-water interface [2, 67]. The ζ-potential of the

DOI: 10.7569/RAA.2019.097314

air-water interface ranges from -110 mV at pH 10.5 to 20 mV at pH of 2 or 3 with a typical ζ-potential value of -65 mV commonly used for neutral water. There is a general trend of negative ζ-potential at higher pH and positive ζ-potential at low pH (Figure 9). The ζ-potential is also influenced by ionic strength. High ironic strength compresses the double layer and decreases the ζ-potential [64]. The ζ-potential plays the key role in the determination of repulsive electrical double layer forces. Once the repulsive electrical double layer forces are overcome, hydration forces will result in the colloid and bacterial adhesion. Most of the adhesion observations indicate that adhesion of colloids and bacteria at the air-water interface depends on the solution hydrophobicity, which is greatly influenced by the presence of surfactants in the solution [90].

3.2.3 Impact of Surfactants

Air-water interfacial tension as well as water-porous medium interfacial tension can be lowered in the presence of surface active agents, or surfactants [91]. Surfactants are amphiphilic compounds, containing a hydrophobic tail and a hydrophilic head. The hydrophilic head can be either negatively, positively, dually or neutrally charged (Figure 10). Correspondingly, the surfactants are classified as anionic, cationic, zwitterionic or nonionic surfactants [92]. Anionic surfactants such as sulfates, sulfonates, and gluconates tend to create foam and are popularly

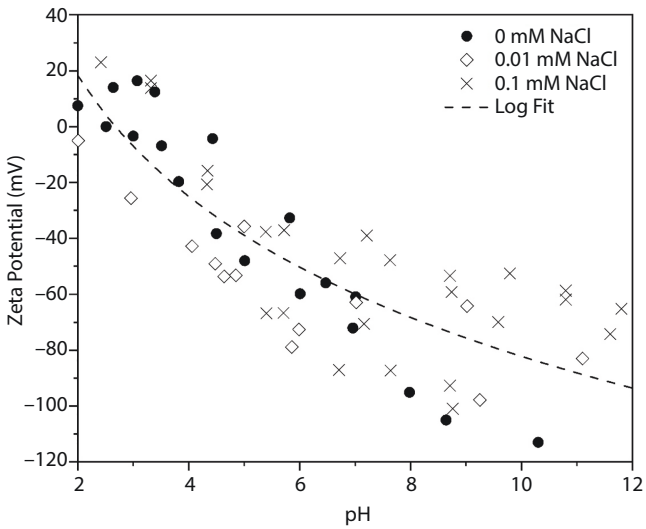

Figure 9 ζ-Potential of the Air-Water Interface as a Function of Solution pH. The ζ-potential of the air-water interface ranges from -110 mV at pH 10.5 to 20 mV at pH of 2 or 3 with a typical ζ-potential value of -65 mV commonly used for neutral water. There is a general trend of negative ζ-potential at higher pH and positive ζ-potential at low pH.

DOI: 10.7569/RAA.2019.097314

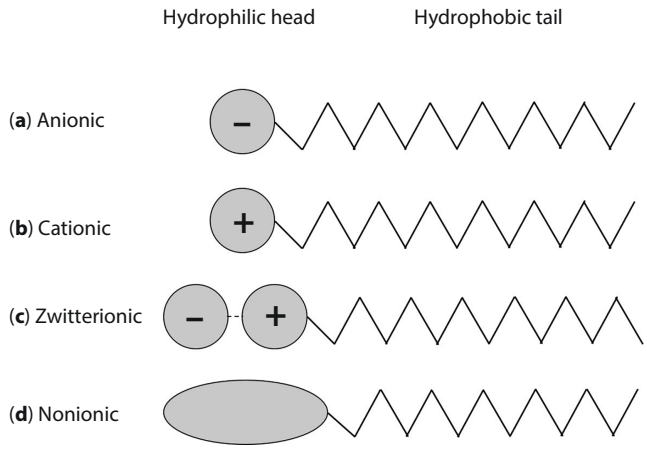

Figure 10 Illustration of Anionic, Cationic, Zwitterionic and Nonionic Surfactants. Surfactants are amphiphilic compounds, containing a hydrophobic tail and a hydrophilic head. The hydrophilic head can be either negatively, positively, dually or neutrally charged. Correspondingly, the surfactants are classified as (a) anionic, (b) cationic, (c) zwitterionic, and (d) nonionic surfactants.

used for lifting and suspending colloids [93]. Cationic surfactants such as alkyl ammonium chlorides are commonly used in antistatic products such as fabric softeners and antimicrobial agents such as disinfectants [94]. It should be noted that anionic surfactants cannot work together with cationic surfactants as they may fall out of solution owing to charge neutralization. Zwitterionic surfactants have both positive and negative charges on their hydrophilic heads, which cancel each other to create a net zero charge. Solution pH thus plays a key role in the performance of zwitterionic surfactants. In acidic solutions, the zwitterionic surfactants are positively charged, acting as cationic surfactants. In alkaline solutions, they act as anionic surfactants by developing negative charges. Zwitterionic surfactants are commonly used in personal care products such as shampoos and cosmetics [95]. Nonionic surfactants such as ethoxylates, alkoxylates, and cocamides can be non-foaming or low-foaming, and are good at emulsifying oils [96]. Nonionic surfactants can be used together with anionic surfactants to create dual-action, multi-purpose cleaners that can not only lift and suspend colloids, but also emulsify oily soils [97]. The decrease of surface tension in the presence of surfactants is described by the Szyszkowski equation [98]:

$$\gamma = \gamma_0 \left[1 - BLn\left(1 + \frac{C}{A} \right) \right] \tag{34}$$

DOI: 10.7569/RAA.2019.097314

where γ_0 is the interfacial tension in the absence of surfactant (e.g., the surface tension of pure water), C is the surfactant concentration, and A and B are variables related to properties of the surfactant.

3.2.4 Air-Water Interface in a Porous Medium

In the subsurface soil, the air-water interface is created by the trapped air in the pore space, which plays an important role in the fate and transport of colloids and bacteria in the porous media by creating an extra sink to adsorb not only hydrophobic particles but also hydrophilic ones [99]. The degree of adhesion at the air-water interface is controlled by the colloid and bacterial surface hydrophobicity, solution ionic strength, and surface charges, etc. Adhesion of colloids and bacteria increases with the increase of colloid and bacterial hydrophobicity and solution ionic strength [100]. In addition, positively charged colloids have very strong affinity to the air-water interface since the air-water interface is negatively charged [101]. Similarly to adhesion of hydrophobic substances at the air-water interface, adhesion of colloids and bacteria to the air-water interface is essentially irreversible, in that the capillary forces hold them on the air-water interface after the rupture [64, 67].

The air-water interface complicates the fate and transport of colloids and bacteria in the subsurface soil. Since the very specific molecular properties of the air-water interface differ from those of the bulk solution, air-water interface may retain colloids and bacteria [102]. Air at the air-water interface behaves like a flat hydrophobic surface, making the air-water interface attractive to hydrophobic substances. In addition, because of the capillary forces, the adsorption of hydrophobic substances to the air-water interface is essentially irreversible. This preferential and irreversible adsorption at the air-water interface strongly influences the movement and spatial distribution of hydrophobic substances including microorganisms [103]. The water surface tension is influenced by the pH of water. The electrokinetic data indicate that the isoelectric point of the air-water interface is pH 3.8, at which the air-water interface exhibits a minimum surface tension [104]. Also, ions are not distributed equally between the air-water interface and the bulk solution. At the air-water interface, a significantly higher concentration of ions accumulates as compared to the bulk phase, which is reflected by the ionization equilibrium constant obtained from the surface and electrokinetic potential data [105]. Specifically, hydrogen and hydroxide ions have higher tendency to accumulate at the air-water interface than in the bulk solution, with hydroxide ions being more pronounced. The accumulation of ions at the air-water interface is reflected in ζ-potential, another important physicochemical parameter that is commonly used to describe the adsorption at the air-water interface [106]. ζ-potential is a function of surface conductivity and is induced by the air and the excess electrical charges at the interface. The protons or hydrogen ions adsorb on the air-water

DOI: 10.7569/RAA.2019.097314

interface, outside of which is a diffuse layer. ζ-potential can be quantified by the electrical potential at the Stern layer [107].

At the air-water interface, free O-H groups of water account for 28% of the interfacial water [108, 109]. Lack of polarizability at the air-water interface induces the accumulation of large, unfavorable anions with high electrostatic potentials at the interface. Consequently, surface tension of salt solutions increases with the increase of solution ionic strength [110]. The free energy changes due to anion adsorption at the air-water interface is dominated by a balance between favorable cavitation and unfavorable desolvation, which moves an anion from bulk to the air-water interface. The shift of anions also reduces the favorable interactions of the anion with the solvation shell [111]. Anions adsorb more strongly to the air-water interface than their counterpart cations. Subsequently, electrical double layer is formed near the interface, with the anions residing in or near the topmost layer of the solution and the cations residing below the anions [112, 113]. In salt solutions that contain alkali metal cations, the cations are excluded from the topmost layer [114]. Compared with anions, adsorption of cations is less pronounced and its effects on the air-water interface property are generally weak. However, cations affect the strength of the electrical double layer, which, in turn, influences the ion distribution at the air-water interface [113].

3.2.5 Force Balance at the Air-Water Interface

Interactions between colloids and bacteria and the air-water interface also begin with the long-range, non-specific electrical double layer forces and Lifshitz–van der Waals forces, which dominate over short-range hydration forces when the separation distance between colloids or bacteria and the air-water interface is greater than a few hundred nanometers. Colloids, bacteria and the air-water interface are negatively charged. Thus, the electrical double layer forces are repulsive. Although the Lifshitz–van der Waals forces are attractive, the net interactions are repulsive at this stage since electrical double layer forces are much stronger than the Lifshitz–van der Waals forces, which prevents colloids and bacteria from getting close to the air-water interface. With the help of hydrodynamics, colloids and bacteria may overcome the repulsive force barrier to further decrease the separation distance, leading to the domination of hydration forces. At the equilibrium separation distance, where the physical contact can occur, adhesion is possible when the net force is negative. This is possible owing to the double layer superimposition and subsequent significantly decreased electrical double layer forces. The dominating hydration forces are specific interactions in close proximity to the air-water interface since the hydration forces reflect the potential bonding induced by the electron-donor (i.e., hydrogen-acceptor) and electron-acceptor (i.e., hydrogen-donor). Owing to the accumulation of OH^- groups at the air-water interface, the air-water interface serves as the electron-donor (i.e., hydrogen-acceptor) and the colloids or bacteria serve as the electron-acceptor (i.e., hydrogen-donor). The hydration forces are strong enough to establish stable attachment of the colloids and bacteria to the interface.

DOI: 10.7569/RAA.2019.097314

The adhesion of colloids and bacteria to the air-water interface is also influenced by solution chemistry such as ionic strength and pH. At low ionic strength, the repulsive electrical double layer forces are strong to prevent them from adhering. Adhesion is more possible at high ionic strength that leads to the compression of the electrical double layers. Similarly, at high pH, the high OH^- concentration in the solution enhances the repulsive interactions between colloids or bacteria with the air-water interface. On the contrary, at low pH, the reduced OH^- accumulation at the air-water interface owing to the neutralization by H^+ enhances adhesion.

3.2.6 Impact of Air-Water Interface on Adhesion to Porous Media

In the subsurface environment, colloids and bacteria are affixed to the porous media by capillary forces. The air-water interface forms a water bridge between colloids or bacteria and the porous medium surface (Figure 11). Depending on the water content in the porous media, the water bridge may shrink or expand to

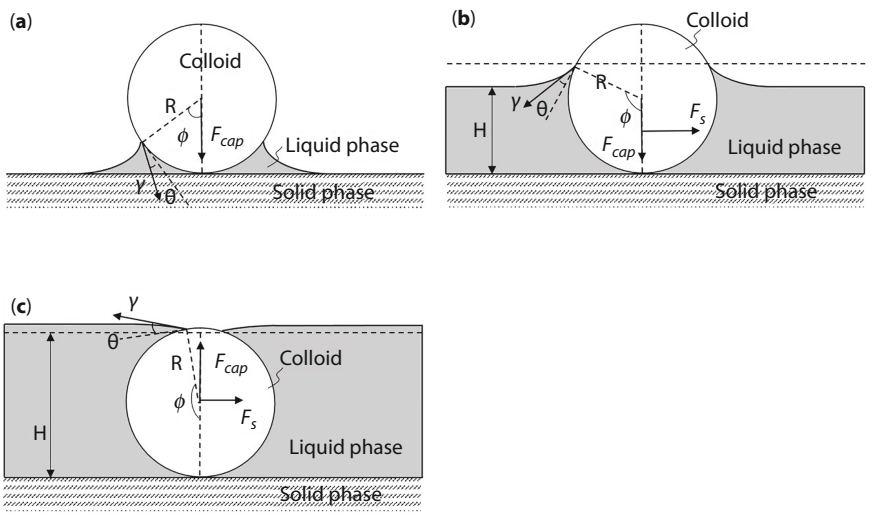

Figure 11 Schematic of Colloids and Bacteria Interactions with the Air-Water Interface. The air-water interface forms a water bridge between colloids or bacteria and the porous medium surface. Depending on the water content in the porous medium, the water bridge may shrink or expand to submerge the porous medium and capillary forces affix colloids or bacteria to the porous medium. With the increase of water content, water level increases and the air-water curvature changes from concave to convex, at this point the capillary force lifts colloids or bacteria from the porous medium: (a) small water content; (b) intermediate water content; and (c) large water content. R is the radius of the colloids or bacteria, γ is the water surface tension, ϕ is the filling angle between the center of the colloids or bacteria and the water contact line, θ is the colloid or bacterial water contact angle, F_{cap} is the capillary force, F_s is the shear force, and H is the thickness of water film.

DOI: 10.7569/RAA.2019.097314

submerge the porous media and capillary forces affix colloids or bacteria to the porous media. With the increase of water content, water level increases and the air-water curvature changes from concave to convex, at this point the capillary force lifts colloids or bacteria from the porous media. The capillary forces between colloids and bacteria and the porous media when a meniscus is formed are calculated by:

$$F_{cap} = 2\pi R\gamma \, sin\phi \, sin(\phi + \theta) + \Delta p \pi R^2 \, sin^2 \, \phi \tag{35}$$

where R is the radius of the colloids or bacteria, γ is the water surface tension, ϕ is the filling angle (degree) between the center of the colloids or bacteria and the water contact line, θ is the colloid or bacterial water contact angle, and Δp is the capillary pressure. In combination with the Young-Laplace equation, the capillary forces are expressed as:

$$F_{cap} = \pi R\gamma \, [2\sin \phi \, \sin(\phi + \theta) + cos\theta(1 + \cos \phi)^2 - \sin \phi] \tag{36}$$

Affixed colloids or bacteria can be released from porous media by rolling, the detachment criterion for which is given by the torque balance:

$$1.399 F_s \frac{H}{2} = F_{cap} RSin\phi \tag{37}$$

where H is thickness of water film and F_s is the shear force, which is calculated as [115]:

$$F_s = 1.7(6\pi)\mu \frac{H}{2} v \tag{38}$$

where μ is water dynamic viscosity, v is the water flow velocity measured at the distance H/2 from the surface of the pore wall. If colloids or bacteria are completely covered with water, then H/2 = R. If the left-hand-side of equation (38) is larger than the right-hand-side, the colloids or bacteria are removed from the porous media.

4. Adhesion Theory Implementations

4.1 Water Saturation and Air-Water Interface in Porous Media

Under unsaturated flow conditions, trapped air in the porous media may serve as an additional adsorption sink for attachment, which is not evenly distributed

DOI: 10.7569/RAA.2019.097314

along the length of the porous medium. In practice, the distribution of the air-water interface in the porous media can be estimated from the pore size radius [116]:

$$S_0 = \frac{\rho_0 g}{\alpha\gamma}\int_{\theta_c}^{\theta_0}\left[\left(\frac{\theta_c}{\theta_0}\right)^{\frac{n}{1-n}} - 1\right]^{\frac{1}{n}} d\theta_c \tag{39}$$

where S_0 is the air-water interfacial area, ρ_0 is the water density, g is the gravitational constant, γ is the water surface tension, α is the inverse of the air-entry potential, θ_c is the volumetric water content, θ_0 is the total pore volume of the porous medium, and n is the parameter related to pore size distribution. The air-water interfacial area decreases with increasing water saturation.

4.2 Liquid-Gas-Solid Three-Phase Interface and Particle Transport

The liquid-gas-solid three-phase interface is a common phenomenon in the subsurface soil, where the mobile particles such as colloids or bacteria are retained [3]. Mathematical models have been developed to describe particles based on the advection-dispersion equation. Currently, most of the available transport models are developed based on colloid transport observations. Though biological colloids (e.g., bacteria) and non-biological colloids (e.g., mineral colloids) differ in terms of potential physiological controls and polymeric material contributions, their transport behaviors in environmental porous media share important similarities. The most fundamental similarity is that they undergo deposition in porous media, which is usually described with the filtration theory and formulated as first-order kinetics [3]. Recent advances in colloid transport modeling have been made by considering two-site/two-region attachment [117, 118], Langmuir-type reaction kinetics [119, 120], random sequential adsorption blocking [121], and solid phase heterogeneity [122]. In these models, the system is considered to consist of three phases, a solution phase, a mobile solid phase, and an immobile solid phase. The interactions between the three phases are governed by mass balance considerations and are described by first- or second-order reactions. Successful applications of these types of models have been observed in laboratory column studies [123].

Most of these models are based on steady-state saturated flow conditions. Transport under unsaturated conditions differs considerably from transport under saturated conditions, as demonstrated by previous research [124–126]. To address unsaturated colloid and bacterial transport, air-phase has been introduced as an additional adsorption site. So far, successful attempts have been made to quantify and predict colloid and bacterial transport under unsaturated water flow

DOI: 10.7569/RAA.2019.097314

conditions or in the presence of the air-water interface [13, 124, 125, 127-132]. During transport, colloid and bacterial adhesion is assumed to occur at the porous media by physicochemical deposition, at the air-water interface owing to capillary forces, or in small pore throats at the air-water-porous medium three-phase interface due to physical constraints. Recent studies show that colloid and bacterial adhesion at the air-water-porous media three-phase interfaces plays the key role in their retention in the pore system [6, 12, 65, 66, 133–137]. Subsequently, the modeling approach assumes that the adhesion occurs at the air-water-porous media three-phase interface:

$$\frac{\partial}{\partial t}[\theta_c C] = \frac{\partial}{\partial Z}\left[D_Z \theta_c \frac{\partial C}{\partial Z} \right] - \frac{\partial}{\partial Z}[qC] - k_d \theta_c C + k_{des} \rho_b S \tag{40}$$

$$\frac{\partial S}{\partial t} = k_d \frac{\theta_c}{\rho_b} C - k_{des} S \tag{41}$$

where C is the particle concentration in the liquid phase, D_z is the apparent dispersion coefficient, θ_c is the volumetric water content, q is the specific discharge (Darcian fluid flux), k_d is the deposition coefficient at the liquid-gas-solid interface, k_{des} is desorption coefficient, ρ_b is the bulk density, S is the retained particles expressed in terms of per solid mass, z is the axial coordinate, and t is time.

In the above models, colloid and bacterial deposition rate is usually considered to be constant along the depth of the soil, which is true under favorable attachment conditions [125, 131]. Consequently, colloid and bacterial concentration would display exponential decrease with the travel distance. However, a growing body of laboratory scale column experiments suggests that the retained colloid and bacterial profiles decay nonexponentially under unfavorable attachment conditions, i.e., low ionic strength. Reported differences in deposition profile shapes under unfavorable attachment conditions indicate apparent decreases in deposition rate coefficients with the transport distance, which is attributed to variations in pore structures, grain size, hydrodynamics and solution chemistry [138–141]. The mean aqueous and colloid and bacterial concentrations at a given depth and time can thus be determined for two log-normally distributed parameters k_d and k_{des} as:

$$\langle C(z,t) \rangle = \iint_0^\infty C(z,t,k_d,k_{des}) F(k_d,k_{des}) dk_d\, dk_{des} \tag{42}$$

DOI: 10.7569/RAA.2019.097314

$$\left\langle S(z,t)\right\rangle = \iint_{0}^{\infty} S(z,t,k_d,k_{des})F(k_d,k_{des})dk_d\,dk_{des} \tag{43}$$

where $C(z, t, k_d, k_{des})$ and $S(z, t, k_d, k_{des})$ are the aqueous and solid phase particle concentrations.

4.3 Force Quantification

In the porous media, the mobilization of colloids and bacteria is very important since it can lead to the porous media physical and chemical changes. The colloid and bacterial transport is influenced by their surface thermodynamic properties. However, the quantitative influence is not currently clear [6, 49]. By introducing the interface variables into the Gibbs free energy and combining with Young-Laplace equation, the surface thermodynamic properties including surface free energy, surface enthalpy, and surface entropy are linked to the size and shape of the colloids and bacteria. The thus theoretically estimated surface thermodynamic properties are consistent with experimental values [142]. Typically, for colloids larger than 10 nm, the surface thermodynamic properties vary linearly with the reciprocal of the colloid size. However, for colloids smaller than 10 nm, the colloid size has much more significant influence on the surface thermodynamic properties of the colloids, which do not follow linear relationship.

Figure 12 shows the four scenarios of colloids and bacteria attachment at the air-water-porous media three-phase interface: (a) colloids or bacteria do not attach to either the air-water interface or the porous media owing to repulsive interactions with both the air-water interface and the porous media, (b) colloid or bacteria attach to the porous media owing to repulsive interactions with the air-water interface and attractive interactions with the porous media, (c) colloids or bacteria attach to the air-water interface owing to the attractive interactions with the air-water interface and repulsive interactions with the porous media, and (d) colloid or bacteria attach to both the air-water interface and the porous media owing to attractive interactions with both the air-water interface and the porous media. For the above interactions, Lifshitz-van der Waals (*LW*), Lewis acid/base and electrostatic forces are considered [56]. The distance-dependent Lifshitz–van der Waals interaction free energy, ΔG_{132}^{LW} between a spherical-shaped particle, 1, and a flat plate of the liquid-gas interface or sediment surface, 2, immersed in water, 3, is calculated by [10]:

$$\Delta G_{132}^{LW}(sphere-plate) = \frac{A}{6}\left[\frac{2R^2}{y(4R+y)} + \frac{2R^2}{(2R+y)^2} + ln\frac{y(4R+y)}{(2R+y)^2}\right] \tag{44}$$

DOI: 10.7569/RAA.2019.097314

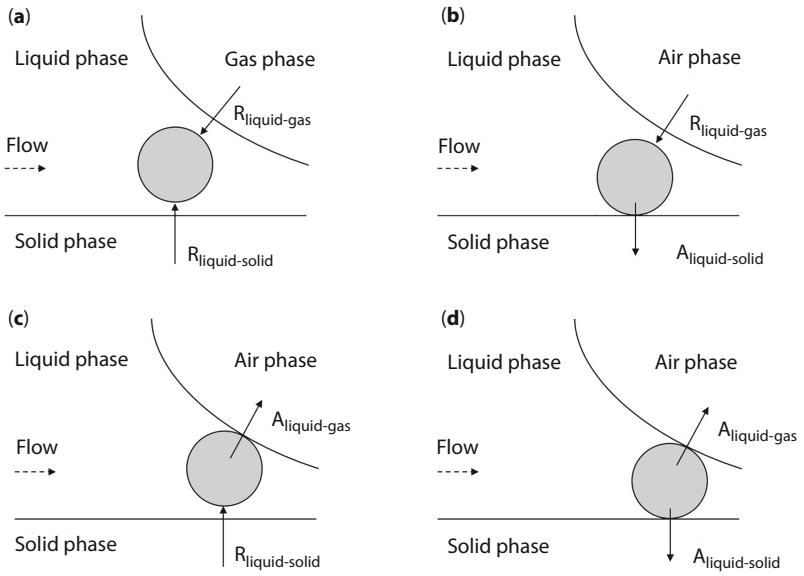

Figure 12 Four Scenarios of Particle Attachment at the Liquid-Gas-Solid Three-Phase Interface. (a) Colloids or bacteria do not attach to either the air-water interface or the porous medium; (b) Colloid or bacteria attach to the porous medium; (c) Colloids or bacteria attach to the air-water interface; and (d) Colloid or bacteria attach to both the air-water interface and the porous medium.

where R is the radius of the particle, y is the separation distance between the particle and the flat plate of the liquid-gas interface or sediment surface, and A is the Hamaker constant, which can be obtained by:

$$A = 24\pi y_0^2 \left(\sqrt{\gamma_3^{LW}} - \sqrt{\gamma_2^{LW}}\right)\left(\sqrt{\gamma_3^{LW}} - \sqrt{\gamma_1^{LW}}\right) \tag{45}$$

where y_0 is the equilibrium separation distance of 1.57 Å.

The distance-dependent Lewis acid/base interaction free energy, ΔG_{132}^{AB} between a spherical-shaped particle, 1, and a flat plate of the liquid-gas interface or sediment surface, 2, immersed in water, 3, is calculated by [10]:

$$\Delta G_{132}^{AB} = 2\pi R y_0 \Delta G_{y_0 132}^{AB} e^{(y_0 - y)/\lambda} \tag{46}$$

where λ is the water decay length (i.e., 0.6 nm for pure water) and $\Delta G_{y_{0132}}^{AB}$ is the Lewis acid/base interaction free energy of two parallel plates, 1 and 2, immersed in water 3, at the equilibrium distance [10]:

DOI: 10.7569/RAA.2019.097314

$$\Delta G_{y_0 132}^{AB} = 2\left[\sqrt{\gamma_3^+}\left(\sqrt{\gamma_1^-}+\sqrt{\gamma_2^-}-\sqrt{\gamma_3^-}\right)+\sqrt{\gamma_3^-}\left(\sqrt{\gamma_1^+}+\sqrt{\gamma_2^+}-\sqrt{\gamma_3^+}\right)-\sqrt{\gamma_1^+\gamma_2^-}-\sqrt{\gamma_1^-\gamma_2^+}\right] \quad (47)$$

The distance-dependent electrostatic interaction free energy, ΔG_{132}^{EL} between a spherical-shaped particle, 1, and a flat plate of the liquid-gas interface or sediment surface, 2, immersed in water, 3, is calculated by [10]:

$$\Delta G_{132}^{EL} = \pi\varepsilon\varepsilon_0 \frac{R}{y}\left[2\psi_1\psi_2 Ln\left(\frac{1+e^{-\kappa y}}{1-e^{-\kappa y}}\right)+\left(\psi_1^2+\psi_2^2\right)Ln(1-e^{-2\kappa y})\right] \quad (48)$$

where ε and ε_0 are the relative dielectric permittivity of water and permittivity under vacuum, $1/\kappa$ is the Debye-Hückel length, which is also an estimation of the effective thickness of the electrical double layer, and ψ_1 and ψ_2 are potentials at the colloid or bacterial surface and the porous medium surface [37]:

$$\psi_0 = \zeta\left(1+\frac{z}{R}\right)\exp(\kappa z) \quad (49)$$

where ζ is the zeta potential measured at the slip plane, z is the distance from the particle surface to the slip plane, which is usually in the range of 0.3 nm to 0.5 nm. The κ value in the above equations is estimated by [10]:

$$\kappa = \sqrt{4\pi e^2 \sum_i \frac{\upsilon_i^2 n_i^2}{\varepsilon\varepsilon_0 k_B T}} \quad (50)$$

where e is the charge of the electron, υ_i is the valence of each ionic species, n_i is the number concentration of ions of each species in the bulk liquid, k_B is the Boltzmann constant, and T is the absolute temperature.

4.4 *Atomic Force Microscopy Measurements*

Atomic force microscopy force measurements are now commonly used to quantify the interactions of colloids and bacteria immobilized on a gelatin-treated silicon nitride V-shaped cantilever probe [143]. To maintain the original structure and

DOI: 10.7569/RAA.2019.097314

integrity of colloid and bacteria, especially bacteria, force measurements are usually conducted immediately after the immobilization process. The force-distance curves are obtained for both the approaching and retracting motions of the tip [144]. In the retraction phase, the pull-off occurs at the location where the cantilever elastic stress overcomes the adhesive interactions between colloid or bacteria and the substrate, which is used as a key parameter to evaluate colloid and bacterial adhesion (Figure 13). Force-distance curves are generated with data being processed using related software from the deflection versus piezo position for each cycle, which includes approaching the substrate surface with the cantilever probe, contacting the surface, and retracting from the contact.

4.5 Linkage of Interactions and Transport

The above interactions are responsible for k_d and k_{des} defined in the colloid and bacterial transport models. They can be assumed to be log-normal stochastic parameters, which are correlated. In practice, a joint probability density function is used to quantify the correlation [145]:

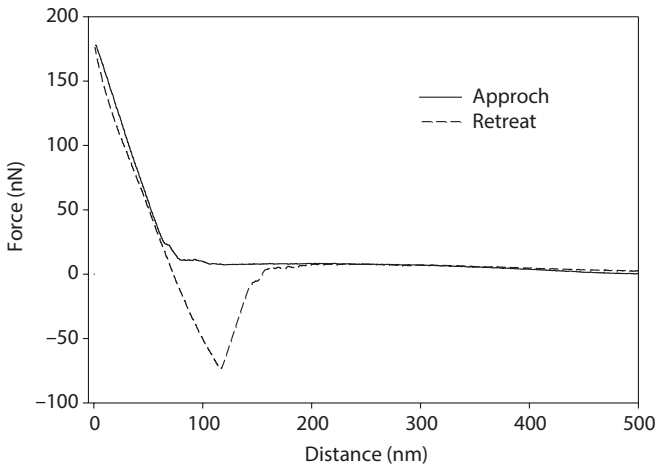

Figure 13 Interaction Measurements by AFM. The force-distance curves are obtained for both the approaching and retracting motions of the tip on colloids or bacteria. In the retraction phase, the pull-off occurs at the location where the cantilever elastic stress overcomes the adhesive interactions between colloid or bacteria and the substrate, which is used as a key parameter to evaluate colloid and bacterial adhesion. Force-distance curves are generated with data from the deflection versus piezo position for each cycle, which includes approaching the substrate surface with the cantilever probe, contacting the surface, and retracting from the contact.

DOI: 10.7569/RAA.2019.097314

$$F(k_d, k_{des}) = \frac{1}{2\pi\sigma_d\sigma_{des}k_d k_{des}\sqrt{1-\rho_{dr}^2}} \exp\left[-\frac{Y_d^2 - 2\rho_{dr}Y_d Y_{des} + Y_{des}^2}{2\left(1-\rho_{dr}^2\right)}\right] \tag{51}$$

where σ_d and σ_{des} are the standard deviations of the log-normal probability density functions for k_d and k_{des} respectively; Y_d and Y_{des} are the normalized log-transformed variables and are defined as:

$$Y_d = \frac{Ln(k_d) - \mu_d}{\sigma_d} \tag{52}$$

$$Y_{des} = \frac{Ln(k_{des}) - \mu_{des}}{\sigma_{des}} \tag{53}$$

Here μ_d and μ_{des} are the mean values of the log-normal probability density function, i.e.,

$$\mu_d = Ln\left(\langle k_d \rangle - 0.5\sigma_d^2\right) \tag{54}$$

$$\mu_{des} = Ln\left(\langle k_{des} \rangle - 0.5\sigma_{des}^2\right) \tag{55}$$

where $<k_d>$ and $<k_{des}>$ are the ensemble average of k_d and k_{des} respectively. The parameter ρ_{dr} is the correlation coefficient between Y_d and Y_{des} and is defined as:

$$\rho_{dr} = Y_d Y_{des} = \int_0^\infty\int_0^\infty Y_d Y_{des} F(k_d, k_{des}) dk_d\, dk_{des} \tag{56}$$

$\rho_{dr} = 1$ when Y_d and Y_{des} are perfectly correlated; $\rho_{dr} = 0$ when Y_d and Y_{des} are uncorrelated; and $\rho_{dr} = -1$ when Y_d and Y_{des} are perfectly inversely correlated.

DOI: 10.7569/RAA.2019.097314

4.6 Surfactant Attachment at the Air-Water Interface

Adhesion theory can also be applied to adhesion of surfactants at the air-water interface. Surfactants preferably adsorb at the interfaces energetically, which decreases the interfacial tension. The more the surfactants are adsorbed at the interface, the greater the decrease of the interfacial tension is [146]. Once the interface is saturated with surfactants, the interfacial tension will not be decreased any further. Instead, surfactants form micelles in the solution phase [147]. The self-association or micellization is initiated by the amphiphilic character of the surfactants, whereby the hydrophobic portion forms the micelle core (known as normal micelle) and the polar head groups form the micelle-water interface (Figure 14a). Micelles are formed when the surfactant concentration is greater than the critical micelle concentration (cmc), which is a function of the surfactant structure, composition, temperature, ionic strength, and the presence and types of organic additives in the solution [147].

The minimization of the unfavorable contact between nonpolar surfactantchains and the polar solvent compensates the loss of entropy by micelle formation [148]. In addition to the normal micelles, inverse micelles also exist which cluster their headgroups and orient their chains towards a surrounding nonpolar phase (Figure 14b). The interfacial activity and amphiphilic nature of the surfactant molecules render them adsorbable to the aquifer media, reducing the interfacial tension.

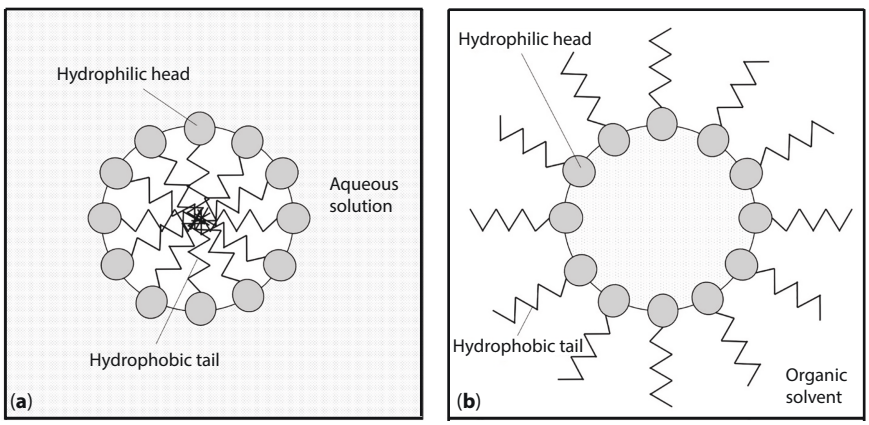

Figure 14 Surfactant Micelle Formation. Once the interface is saturated with surfactants, surfactants form micelles in the solution phase: (a) The self-association or micellization is initiated by the amphiphilic character of the surfactants, whereby the hydrophobic portion forms the micelle core (known as normal micelle) and the polar head groups form the micelle-water interface and (b) Inverse micelles are formed which cluster their headgroups and orient their chains towards a surrounding nonpolar phase.

DOI: 10.7569/RAA.2019.097314

They are subsequently commonly used in contaminated soil remediation [149]. Surfactant micellization, surfactant adsorption on aquifer media and formation of admicelles/hemimicelles, contaminant micellar-solubilization, middle-phase micromulsion formation, contaminant adsorption on aquifer media, and contaminant adsorption on admicelles/hemimicelles (adsolubilization) occur during surfactant applications [149]. It should be noted that while extra-micellar contaminants can be adsorbed directly, micellar-solubilized contaminants must partition out of micelles before being adsorbed [148].

Combining the Lifshitz-van der Waals interactions and Lewis acid/base interactions, surfactant behavior in solution can be quantitatively interpreted. Using poly(ethylene oxide) (POE) surfactants as an example, γ^{LW} of POE surfactants is in the range of 20.6 mN/m to 21.3 mN/m, which increases with the increase of POE chain length. When POE surfactants are applied at low concentrations, a very compact monolayer can be formed at the interface with an interfacial volume fraction close to unity and the accumulation of the surfactants at the interface following the Frumkin adsorption isotherm [150]. Mathematically, the relationship of surface tension decrease in the presence of surfactants can be related to Gibbs free energy of the interactions between surfactant molecules. Specifically, with the increase of surfactant concentration, the micelles are formed when the concentration reaches the cmc, which is attributed to hydrophobic interactions between amphiphilic surfactant molecules [151]:

$$\Delta G_{131}^{TOT} A = kTLn(cmc) \tag{57}$$

where ΔG_{131}^{TOT} is the interaction free energy between surfactant molecules, A is the limiting area per surfactant molecule, k is the Boltzmann constant, and T is the absolute temperature. For POE surfactants, the limiting area per surfactant molecule, A can be estimated by:

$$\frac{A}{N^{\frac{6}{11}}} \cong \left(\frac{a^{\frac{5}{3}} kT}{\gamma} \right)^{\frac{6}{11}} \tag{58}$$

where γ is the liquid surface tension when saturated with the POE surfactants, N is the number of ethylene oxide segments in the surfactant tails, and a is the effective monomer size, which is assumed to be 2.1 Å [151].
ΔG_{131}^{TOT} is the sum of Lifshitz-van der Waals interaction and Lewis acid/base interaction free energies, which can be calculated based on the surfactant and liquid surface thermodynamic properties [152]:

DOI: 10.7569/RAA.2019.097314

$$\Delta G_{131}^{TOT} = \Delta G_{131}^{LW} + \Delta G_{131}^{AB} \tag{59}$$

$$\Delta G_{131}^{LW} = -2\left(\sqrt{\gamma_3^{LW}} - \sqrt{\gamma_1^{LW}}\right)^2 \tag{60}$$

$$\Delta G_{131}^{AB} = -4\left(\sqrt{\gamma_1^{+}} - \sqrt{\gamma_3^{+}}\right)\left(\sqrt{\gamma_1^{-}} - \sqrt{\gamma_3^{-}}\right) \tag{61}$$

where ΔG_{131}^{LW} is the Lifshitz-van der Waals interaction free energy, ΔG_{131}^{AB} is the Lewis acid/base interaction free energy. In the above equations, subscript "1" denotes the surfactant and "3" denotes the liquid.

ΔG_{131}^{LW} is typically one order of magnitude greater than ΔG_{131}^{AB}. Thus ΔG_{131}^{LW} is usually the driving force in determining the cmc of the surfactants. Lifshitz-van der Waals forces include Keesom, Debye, and London interactions. Of these three, Keesom and Debye interactions are only found among molecules that have permanent dipole moments. The London interactions, however, are universal and are of preponderate importance especially in aqueous media that contain electrolytes [152]. Therefore, the Lifshitz–van der Waals surface tension component, γ^{LW} based on which intermolecular Lifshitz–van der Waals interactions are calculated, and are mainly contributed by the London interactions. Owing to the induced dipole potential, Lifshitz–van der Waals interactions occur between two surfactant molecules.

5. Summary

This review revisits the colloid and bacterial adhesion theory and uses the adhesion theory to interpret colloid and bacterial transport in porous media. Adhesion of colloids and bacteria to porous media or the air-water interface is attributed to their interactions with the surfaces or the interface, which include Lifshitz-van der Waals forces, Lewis acid/base forces, hydration forces, and electrical double layer forces. In the presence of air-water interface, colloids and bacteria are also subject to the capillary forces. By introducing the interface variables into the Gibbs free energy and combining with Young-Laplace equation, the surface thermodynamic properties of the colloids and bacteria are quantified. Subsequently, the distance-dependent Lifshitz-van der Waals forces, Lewis acid/base forces, hydration forces, and electrical double layer forces can be calculated, which are then used to interpret colloid and bacterial transport in porous media.

Acknowledgments

The authors acknowledge the support from the National Institute of Food and Agriculture through Grant No. 2018-68002-27920 to Florida A&M University and

DOI: 10.7569/RAA.2019.097314

also the National Science Foundation through Grant No. 1735235 awarded as part of the National Science Foundation Research Traineeship.

References

[1] A. Karnieli, T. Markovich and D. Andelman, Surface pressure of charged colloids at the air/water interface. *Langmuir* **34**, 13322-13332 (2018).
[2] M. Flury and S. Aramrak, Role of air-water interfaces in colloid transport in porous media: A review. *Water Resources Res.* **53**, 5247-5275 (2017).
[3] T.K. Sen and K.C. Khilar, Review on subsurface colloids and colloid-associated contaminant transport in saturated porous media. *Adv. Colloid Interface Sci.* **119**, 71-96 (2006).
[4] V. Guine, J. Martins and J.P. Gaudet, Facilitated transport of heavy metals by bacterial colloids in sand columns. *J. Physique IV France* **107**, 593-596 (2003).
[5] T.D. Scheibe, H.L. Dong and Y.L. Xie, Correlation between bacterial attachment rate coefficients and hydraulic conductivity and its effect on field-scale bacterial transport. *Adv. Water Resources* **30**, 1571-1582 (2007).
[6] G. Chen and M. Flury, Retention of mineral colloids in unsaturated porous media as related to their surface properties. *Colloids Surfaces A* **256**, 207-216 (2005).
[7] S. Park and H.B. Lee, Effect of pH on monolayer properties of colloidal silica particles at the air/water interface. *Colloid Polym. Sci.* **290**, 445-455 (2012).
[8] G. Chen, Bacterial interactions and transport in unsaturated porous media. *Colloids Surfaces B* **67**, 265-271 (2008).
[9] C.J. van Oss, Use of the combined Lifshitz-van der Waals and Lewis acid-base approaches in determining the apolar and polar contributions to surface and interfacial tensions and free energies. *J. Adhesion Sci. Technol.* **16**, 669-677 (2002).
[10] C.J. van Oss, *Interfacial Forces in Aqueous Media*, Marcel Dekker, New York (1994).
[11] Y.X. Luo, H. Li, W.Q. Ding, F.N. Hu and S. Li, Effects of DLVO, hydration and osmotic forces among soil particles on water infiltration. *European J. Soil Sci.* **69**, 710-718 (2018).
[12] S.A. Bradford and S. Torkzaban, Colloid transport and retention in unsaturated porous media: A review of interface-, collector-, and pore-scale processes and models. *Vadose Zone J.* **7**, 667-681 (2008).
[13] G. Gargiulo, S.A. Bradford, J. Simunek, P. Ustohal, H. Vereecken and E. Klumpp, Bacteria transport and deposition under unsaturated flow conditions: The role of water content and bacteria surface hydrophobicity. *Vadose Zone J.* **7**, 406-419 (2008).
[14] J. McGuire and K.R. Swartzel, On the use of water in the measurement of solid-surface tension. *Surface Interface Anal.* **10**, 430-433 (1987).
[15] M.E. Schrader, Contact angle and vapor adsorption. *Langmuir* **12**, 3728-3732 (1996).
[16] N.K. Adam and H.K. Livingston, Contact angles and work of adhesion. *Nature* **182**, 128-128 (1958).
[17] F.M. Etzler, Determination of the surface free energy of solids: A critical review. *Rev. Adhesion Adhesives* **1**, 3-45 (2013).
[18] F.M. Etzler, Characterization of surface free energies and surface chemistry of solids, In: *Contact Angle, Wettability and Adhesion*, Volume 3, K.L. Mittal (Ed.), pp. 219-264, CRC Press, Boca Raton, FL (2003).

DOI: 10.7569/RAA.2019.097314

[19] D. Risovic, A. Penezic, V. Cadez, S. Segota, and B. Gasparovic, Surface free energy tuning of supported mixed lipid layers. *RSC Adv.* **6**, 52475-52484 (2016).
[20] R.J. Good and C.J. van Oss, The modern theory of contact angles and the hydrogen bond components of surface energies, In: *Modern Approaches to Wettability*, M.E. Schrader and G.I. Loeb (Eds.), pp. 1-27, Springer, New York (1992).
[21] T.P. Yin and S. Wu, Compression mechanics of polymer monolayers. *J. Polym. Sci. C*, **34**, 265-271 (1971).
[22] S. Wu, *Polymer Interface and Adhesion*, Marcel Dekker, New York (1982).
[23] G.I. Mantanis and R.A. Young, Wetting of wood. *Wood Sci. Technol.* **31**, 339-353 (1997).
[24] F.L. Leite, C.C. Bueno, A.L. Da Roz, E.C. Ziemath and O.N. Oliveira, Theoretical models for surface forces and adhesion and their measurement using atomic force microscopy. *Intl. J. Molecular Sci.* **13**, 12773-12856 (2012).
[25] Y.J. Dappe, J. Ortega and F. Flores, Weak chemical interaction and van der Waals forces: A combined density functional and intermolecular perturbation theory - Application to graphite and graphitic systems. *Lecture Notes in Physics* **795**, 45-79 (2010).
[26] S. Kawai, A.S. Foster, T. Bjorkman, S. Nowakowska, J. Bjork, F.F. Canova, L.H. Gade T.A. Jung and E. Meyer, van der Waals interactions and the limits of isolated atom models at interfaces. *Nature Commun.* **7**, 11559 (1-7) (2016).
[27] E. Wilhelm, Mitigating complexity: Cohesion parameters and related topics. I: The Hildebrand solubility parameter. *J. Solution Chem.* **47**, 1626-1709 (2018).
[28] C.P. Kelly, C.J. Cramer and D.G. Truhlar, Aqueous solvation free energies of ions and ion-water clusters based on an accurate value for the absolute aqueous solvation free energy of the proton. *J. Phys. Chem. B* **110**, 16066-16081 (2006).
[29] R.D. Hancock and F. Marsicano, Patterns in Lewis acid-vase interactions in aqueous-solution. *South African J. Chem.* **33**, 77-86 (1980).
[30] W.B. Jensen, Lewis acid-base interactions and adhesion theory. *Rubber Chem. Technol.* **55**, 881-901 (1982).
[31] Z.B. Li and B.C.Y. Lu, A molecular model for representing surface tension for polar liquids. *Chem. Eng. Sci.* **56**, 6977-6987 (2001).
[32] A. Bateni, S. Laughton, H. Tavana, S.S. Susnar, A. Amirfazli and A.W. Neumann, Effect of electric fields on contact angle and surface tension of drops. *J. Colloid Interface Sci.* **283**, 215-222 (2005).
[33] Y. Wang, D.K. Sang, Z.J. Du, C. Zhang, M. Tian and J.G. Mi, Interfacial structures, surface tensions, and contact angles of diiodomethane on fluorinated polymers. *J. Phys. Chem. C* **118**, 10143-10152 (2014).
[34] J.N. Israelachvili and R.M. Pashley, Molecular layering of water at surfaces and origin of repulsive hydration forces. *Nature* **306**, 249-250 (1983).
[35] L. Perera, U. Essmann and M.L. Berkowitz, The role of water in hydration force molecular dynamics simulations. *Abstracts Papers Amer. Chem. Soc.* **215**, U185-U185 (1998).
[36] R.P. Misra, S. Das and S.K. Mitra, Electric double layer force between charged surfaces: Effect of solvent polarization. *J. Chem. Phys.* **138**, 114703 (1-9) (2013).
[37] S.S. Dukhin, Nonequilibrium electric surface phenomena. *Adv. Colloid Interface Sci.* **44**, 1-134 (1993).

DOI: 10.7569/RAA.2019.097314

[38] A.J. Babchin, Y. Gur and I.J. Lin, Repulsive interface forces in overlapping electric double-layers in electrolyte-solutions. *Adv. Colloid Interface Sci.* **9**, 105-141 (1978).
[39] W. Silvestre-Alcantara, L.B. Bhuiyan, C.W. Outhwaite and D. Henderson, A modified Poisson-Boltzmann study of the singlet ion distribution at contact with the electrode for a planar electric double layer. *Collection Czechoslovak Chem. Commun.* **75**, 425-446 (2010).
[40] J.Y. Yang, C.Y. Yan, J.C. Huang and Z.H. Li, Numerical solutions of the semiclassical Boltzmann ellipsoidal-statistical kinetic model equation. *Proc. Royal Soc. A* **470**, https://doi.org/10.1098/rspa.2014.0061 (2014).
[41] A.Z. Borucka, J.O.M. Bockris and J.A. Kitchener, Test of the applicability of the Nernst-Einstein equation to self-diffusion and conduction of ions in molten sodium chloride. *J. Chem. Phys.* **24**, 1282-1282 (1956).
[42] C. Hansch and T.E. Klein, Molecular graphics and QSAR in the study of enzyme ligand interactions. On the definition of bioreceptors. *Accounts Chem. Res.* **19**, 392-400 (1986).
[43] H. Gonzalez-Diaz, L. Saiz-Urra, R. Molina and E. Uriarte, Stochastic molecular descriptors for polymers. 2. Spherical truncation of electrostatic interactions on entropy based polymers 3D-QSAR. *Polymer* **46**, 2791-2798 (2005).
[44] M. Recanatini, T.E. Klein, R. Langridge and C. Hansch, Concanavalin X-phenyl beta-D-glucopyranoside interactions. A molecular graphics-QSAR analysis. *Farmaco-Edizione Scientifica* **42**, 879-891 (1987).
[45] W.B. Haines, Studies in the physical properties of soils II A note on the cohesion developed by capillary forces in an ideal soil. *J. Agricultural Sci.* **15**, 529-535 (1925).
[46] P.O. Scheie, The upward force on liquid in a capillary-tube. *Amer. J. Phys.* **57**, 279-280 (1989).
[47] D.B. Asay, M.P. de Boer and S.H. Kim, Equilibrium vapor adsorption and capillary force: Exact Laplace-Young equation solution and circular approximation approaches. *J. Adhesion Sci. Technol.* **24**, 2363-2382 (2010).
[48] M. Mishurov, A. Yakirevich and N. Weisbrod, Colloid transport in a heterogeneous partially saturated sand column. *Environmental Sci. Technol.* **42**, 1066-1071 (2008).
[49] G. Chen, T. Abichou, K. Tawfiq and P.K. Subramaniam, Impact of surface charge density on colloid deposition in unsaturated porous media. *Colloids Surfaces A* **302**, 342-348 (2007).
[50] J.E. Saiers and J.J. Lenhart, Ionic-strength effects on colloid transport and interfacial reactions in partially saturated porous media. *Water Resources Res.* **39**, 1256 (1-13) (2003).
[51] J.J. Lenhart and J.E. Saiers, Colloid mobilization in water-saturated porous media under transient chemical conditions. *Environmental Sci. Technol.* **37**, 2780-2787 (2003).
[52] G. Chen and K.A. Strevett, Microbial surface thermodynamics and interactions in aqueous media. *J. Colloid Interface Sci.* **261**, 283-290 (2003).
[53] G. Chen and K.A. Strevett, Microbial deposition in porous media: A surface thermodynamic investigation. *Environmental Eng. Sci.* **20**, 237-248 (2003).
[54] C.J. van Oss, A. Docoslis and R.F. Giese, The interfacial tensions with water and the Lewis acid-base surface tension parameters of polar organic liquids derived from their aqueous solubilities. *Colloids Surfaces B* **20**, 87-91 (2001).

DOI: 10.7569/RAA.2019.097314

[55] W. Wu, R.F. Giese and C.J. van Oss, Evaluation of the Lifshitz-van der Waals acid-base approach to determine surface-tension components. *Langmuir* **11**, 379-382 (1995).
[56] G. Yang, B. Wang, K. Vu, K. Tawfiq and G. Chen, Role of bacterial adhesion in their subsurface deposition and transport: A critical review. *Rev. Adhesion Adhesives* **3**, 216-252 (2015).
[57] J. Zhuang, N. Goeppert, C. Tu, J. McCarthy, E. Perfect and L. McKay, Colloid transport with wetting fronts: Interactive effects of solution surface tension and ionic strength. *Water Res.* **44**, 1270-1278 (2010).
[58] S.A. Bradford and R.W. Harvey, Future research needs involving pathogens in groundwater. *Hydrogeol. J.* **25**, 931-938 (2017).
[59] C.J. van Oss, Development and applications of the interfacial tension between water and organic or biological surfaces. *Colloids Surfaces B* **54**, 2-9 (2007).
[60] S. Fujii, E. Mouri, K. Akiyama, S. Nakayama, K. Uda, Y. Nakamura and H. Matsuoka, pH-sensitive adsorption behavior of polymer particles at the air-water interface. *Langmuir* **33**, 1451-1459 (2017).
[61] G. Chen and H.L. Zhu, Bacterial adhesion to silica sand as related to Gibbs energy variations. *Colloids Surfaces B* **44**, 41-48 (2005).
[62] S. Patil, J.C. Zhang, K. Tawfiq and G. Chen, Role of interfacial interactions in the deposition of colloidal clay particles in porous media. *J. Adhesion Sci. Technol.* **23**, 1845-1859 (2009).
[63] J.E. Saiers, G.M. Hornberger, D.B. Gower and J.S. Herman, The role of moving air-water interfaces in colloid mobilization within the vadose zone. *Geophysical Res. Letters* **30**, 2083 (1-5) (2003).
[64] J.M. Wan and T.K. Tokunaga, Partitioning of clay colloids at air-water interfaces. *J. Colloid Interface Sci.* **247**, 54-61 (2002).
[65] V. Lazouskaya and Y. Jin, Colloid retention at air-water interface in a capillary channel. *Colloids Surfaces A* **325**, 141-151 (2008).
[66] Y. Zevi, A. Dathe, J.F. McCarthy, B.K. Richards and T.S. Steenhuis, Distribution of colloid particles onto interfaces in partially saturated sand. *Environmental Sci. Technol.* **39**, 7055-7064 (2005).
[67] J.M. Wan and T.K. Tokunaga, Measuring partition coefficients of colloids at air-water interfaces. *Environmental Sci. Technol.* **32**, 3293-3298 (1998).
[68] E.S. Campbell, Hydrogen bonding and the interactions of water molecules. *J. Chem. Phys.* **20**, 1411-1420 (1952).
[69] H.G. Lu, Y.K. Wang, Y.B. Wu, P. Yang, L.M. Li and S.D. Li, Hydrogen-bond network and local structure of liquid water: An atoms-in-molecules perspective. *J. Chem. Phys.* **129**, 124512 (1-5) (2008).
[70] E. Brini, C.J. Fennell, M. Fernandez-Serra, B. Hribar-Lee, M. Luksic and K.A. Dill, How water's properties are encoded in its molecular structure and energies. *Chem. Rev.* **117**, 12385-12414 (2017).
[71] W.F. Claussen, Surface tension and surface structure of water. *Science* **156**, 1226-1227 (1967).
[72] J.M. Berg, J.L. Tymoczko and L. Stryer, *Biochemistry*, W H Freeman, New York (2002).
[73] Y.O. Popov and T.A. Witten, Characteristic angles in the wetting of an angular region: Surface shape. *European Physical J. E* **6**, 211-220 (2001).

DOI: 10.7569/RAA.2019.097314

[74] E. Kuchek and E.V. Gribanova, The acid-base characteristics of the surface of alpha-Al_2O_3: Potentiometry and wetting methods. *Russian J. Phys. Chem. A* **81**, 387-389 (2007).
[75] R. Miller, A. Hofmann, R. Hartmann, K.H. Schano and A. Halbig, Measuring dynamic surface and interfacial-tensions. *Adv. Mater.* **4**, 370-374 (1992).
[76] B. Kronberg, K. Holmberg and B. Lindman, *Surface Chemistry of Surfactants and Polymers*, Wiley, Southern Gate, UK (2014).
[77] A.E. Lutskii, Conjugation properties of functional-groups, participating in formation of intramolecular hydrogen-bond. *Zhurnal Obshchei Khimii* **46**, 1368-1372 (1976).
[78] H. Pauwels and P. Huyskens, Polarity of hydrogen-bonds on carbonyl groups. *Bulletin Psychonomic Soc.* **83**, 427-441 (1974).
[79] L. Paoloni, A. Patti and F. Mangano, Hydrogen-bond with carbonyl groups: Theoretical-study of correlation between X-H stretching frequency-shift and C=O group properties. *J. Molecular Structure* **27**, 123-137 (1975).
[80] C. Laurence, M. Berthelot and M. Helbert, The stereochemistry of hydrogen-bonds on carbonyl groups. *Spectrochim Acta A* **41**, 883-892 (1985).
[81] J. Chen, C.L. Brooks and H.A. Scheraga, Revisiting the carboxylic acid dimers in aqueous solution: Interplay of hydrogen bonding, hydrophobic interactions, and entropy. *J. Phys. Chem. B* **112**, 242-249 (2008).
[82] J. Ni and J.J. Pignatello, Charge-assisted hydrogen bonding as a cohesive force in soil organic matter: Water solubility enhancement by addition of simple carboxylic acids. *Environmental Sci. Processes Impacts* **20**, 1225-1233 (2018).
[83] S. Varghese, S.K. Kannam, J.S. Hansen and P.S. Sathian, Effect of hydrogen bonds on the dielectric properties of interfacial water. *Langmuir* **35**, 8159-8166 (2019).
[84] E.L. Angelina, D.J. Duarte and N.M. Peruchena, Is the decrease of the total electron energy density a covalence indicator in hydrogen and halogen bonds? *J. Molecular Modeling* **19**, 2097-2106 (2013).
[85] L. Guillaumes, P. Salvador and S. Simon, A fuzzy-atom analysis of electron delocalization on hydrogen bonds. *J. Phys. Chem. A* **118**, 1142-1149 (2014).
[86] H.C. Chen, F.D. Mai, B.J. Hwang, M.J. Lee, C.H. Chen, S.H. Wang, H.Y. Tsai, C.P. Yang and Y.C. Liu, Creation of electron-doping liquid water with reduced hydrogen bonds. *Scientific Reports* **6**, 22166 (2016).
[87] D.B. Shear, The generalized Boltzmann distribution. *J. Theoretical Biology* **39**, 165-169 (1973).
[88] M. Meot-Ner, The ionic hydrogen bond. *Chem. Rev.* **105**, 213-284 (2005).
[89] P. Gilli, L. Pretto, V. Bertolasi and G. Gilli, Predicting hydrogen-bond strengths from acid-base molecular properties. The pK(a) slide rule: Toward the solution of a long-lasting problem. *Accounts Chem. Res.* **42**, 33-44 (2009).
[90] I. Svanedal, F. Andersson, E. Hedenstrom, M. Norgren, H. Edlund, S.K. Satija, B. Lindman and A.R. Rennie, Molecular organization of an adsorbed layer: A zwitterionic, pH-sensitive surfactant at the air/water interface. *Langmuir* **32**, 10936-10945 (2016).
[91] W.C. Liao and J.L. Zatz, Surfactant solutions as test liquids for measurement of critical surface-tension. *J. Pharm. Sci.* **68**, 486-488 (1979).
[92] J.G. Feng, Q.C. Chen, X.M. Wu, S.M. Jafari and D.J. McClements, Formulation of oil-in-water emulsions for pesticide applications: Impact of surfactant type and

DOI: 10.7569/RAA.2019.097314

concentration on physical stability. *Environmental Sci. Pollution Res.* **25**, 21742-21751 (2018).
[93] A. Kitahara, K. Watanabe, K. Konno and T. Ishikawa, Mechanism of solubilization of water by oil-soluble surfactant solutions. I. Anionic surfactants. *J. Colloid Interface Sci.* **29**, 48-54 (1969).
[94] A. Kitahara and K. Konno, Mechanism of solubilization of water by oil-soluble surfactant solutions. II. Cationic surfactants. *J. Colloid Interface Sci.* **29**, 1-5 (1969).
[95] Y.M. Xu, X.X. Zhang, X.Q. Zhou, H.Q. Liu and B.C. Xu, Synergistic interactions between zwitterionic surfactants derived from olive oil and an anionic surfactant. *J. Dispersion Sci. Technol.* **40**, 1308-1316 (2019).
[96] T.A. Koretskaya, Influence of foaming on the detergent power of nonionic surfactant solutions. *J. Appl. Chem. USSR* **57**, 2440-2441 (1984).
[97] T. Tamura, Y. Takeuchi and Y. Kaneko, Influence of surfactant structure on the drainage of nonionic surfactant foam films. *J. Colloid Interface Sci.* **206**, 112-121 (1998).
[98] S. Ross and I.D. Morrison, On the alleged ideality of Szyszkowski-Langmuir adsorption. *J. Colloid Interface Sci.* **91**, 244-247 (1983).
[99] V. Lazouskaya, L.P. Wang, H. Gao, X.Y. Shi, K. Czymmek and Y. Jin, Pore-scale investigation of colloid retention and mobilization in the presence of a moving air-water interface. *Vadose Zone J.* **10**, 1250-1260 (2011).
[100] Y. Wen, L.M. Su, W.C. Qin, L. Fu, J. He and Y.H. Zhao, Linear and non-linear relationships between soil sorption and hydrophobicity: Model, validation and influencing factors. *Chemosphere* **86**, 634-640 (2012).
[101] K. Hanni-Ciunel, N. Schelero and R. von Klitzing, Negative charges at the air/water interface and their consequences for aqueous wetting films containing surfactants. *Faraday Discuss* **141**, 41-53 (2009).
[102] F.M. Menger, L. Shi and S.A. Rizvi, Re-evaluating the Gibbs analysis of surface tension at the air/water interface. *J. Amer. Chem. Soc.* **131**, 10380-10381 (2009).
[103] B. Dahlback, M. Hermansson, S. Kjelleberg and B. Norkrans, The hydrophobicity of bacteria: An important factor in their initial adhesion at the air-water-interface. *Archives Microbiol.* **128**, 267-270 (1981).
[104] A.J. Colussi, Can the pH at the air/water interface be different from the pH of bulk water? *Proc. Natl. Acad. Sci. USA* **115**, E7887-E7887 (2018).
[105] R. D'Auria and D.J. Tobias, Relation between surface tension and ion adsorption at the air-water interface: A molecular dynamics simulation study. *J. Phys. Chem. A* **113**, 7286-7293 (2009).
[106] M. Manciu and E. Ruckenstein, Ions near the air/water interface: I. Compatibility of zeta potential and surface tension experiments. *Colloids Surfaces A* **400**, 27-35 (2012).
[107] J.F. Zhang, E. Uchida, K. Suzuki, Y. Uyama and Y. Ikada, Adhesive interaction in water between surfaces with various zeta potentials. *J. Colloid Interface Sci.* **178**, 371-373 (1996).
[108] F.J. Tang, T. Ohto, T. Hasegawa, W.J. Xie, L.M. Xu, M. Bonn and Y. Nagata, Definition of free O-H groups of water at the air-water interface. *J. Chem. Theory Computation* **14**, 357-364 (2018).
[109] C.S. Hsieh, R.K. Campen, M. Okuno, E.H.G. Backus, Y. Nagata and M. Bonn, Mechanism of vibrational energy dissipation of free OH groups at the air-water interface. *Proc. Natl. Acad. Sci. USA* **110**, 18780-18785 (2013).

DOI: 10.7569/RAA.2019.097314

[110] L.A. Bulavin, V.M. Garamus, T.V. Karmazina and E.N. Pivnenko, Measurements of structural and electrostatic parameters and surface tension of micelles of an ionic surfactant versus concentration, ionic strength of solution and temperature by small-angle neutron scattering. *Colloids Surfaces A* **131**, 137-144 (1998).
[111] J.R. Casey, B.J. Schwartz and W.J. Glover, Free energies of cavity and noncavity hydrated electrons near the instantaneous air/water interface. *J. Phys. Chem. Letters* **7**, 3192-3198 (2016).
[112] M.J. Rosen and J.T. Kunjappu, *Surfactants and Interfacial Phenomena*, 4th edition, Wiley, Hoboken, NJ (2012).
[113] E. Clavero and J. Rodriguez, Ionic liquids at the air/water interface. *J. Molecular Liquids* **163**, 64-69 (2011).
[114] P. Jungwirth and D.J. Tobias, Ions at the air/water interface. *J. Phys. Chem. B* **106**, 6361-6373 (2002).
[115] M.M. Sharma, H. Chamoun, D.S.H.S.R. Sarma and R.S. Schechter, Factors controlling the hydrodynamic detachment of particles from surfaces. *J. Colloid Interface Sci.***149**, 121-134 (1992).
[116] J.W. Cary, Estimating the surface-area of fluid-phase interfaces in porous-media. *J. Contaminant Hydrol.* **15**, 243-248 (1994).
[117] J. Simunek, D. Jacques, M.T. van Genuchten and D. Mallants, Multicomponent geochemical transport modeling using HYDRUS-1D and HP1. *J. Amer. Water Resources Assoc.* **42**, 1537-1547 (2006).
[118] J. Simunek, N.J. Jarvis, M.T. van Genuchten and A. Gardenas, Review and comparison of models for describing non-equilibrium and preferential flow and transport in the vadose zone. *J. Hydrol.* **272**, 14-35 (2003).
[119] R. Lindqvist, J.S. Cho and C.G. Enfield, A kinetic-model for cell-density dependent bacterial transport in porous-media. *Water Resources Res.* **30**, 3291-3299 (1994).
[120] J.E. Saiers, G.M. Hornberger and C. Harvey, Colloidal silica transport through structured, heterogeneous porous-media. *J. Hydrol.* **163**, 271-288 (1994).
[121] P.R. Johnson and M. Elimelech, Dynamics of colloid deposition in porous-media - Blocking based on random sequential adsorption. *Langmuir* **11**, 801-812 (1995).
[122] L.F. Song, P.R. Johnson and M. Elimelech, Kinetics of colloid deposition onto heterogeneously charged surfaces in porous-media. *Environmental Sci. Technol.* **28**, 1164-1171 (1994).
[123] G.M. Hornberger, A.L. Mills and J.S. Herman, Bacterial transport in porous-media - Evaluation of a model using laboratory observations. *Water Resources Res.* **28**, 915-923 (1992).
[124] G. Jiang, M.J. Noonan, G.D. Buchan and N. Smith, Transport of *Escherichia coli* through variably saturated sand columns and modeling approaches. *J. Contaminant Hydrol.* **93**, 2-20 (2007).
[125] D. Or, B.F. Smets, J.M. Wraith, A. Dechesne and S.P. Friedman, Physical constraints affecting bacterial habitats and activity in unsaturated porous media: A review. *Adv. Water Resources* **30**, 1505-1527 (2007).
[126] G.M. Jiang, M.J. Noonan, G.D. Buchan and N. Smith, Transport and deposition of *Bacillus subtilis* through an intact soil column. *Australian J. Soil Res.* **43**, 695-703 (2005).
[127] D.K. Powelson and A.L. Mills, Transport of *Escherichia coli* in sand columns with constant and changing water contents. *J. Environmental Quality* **30**, 238-245 (2001).

DOI: 10.7569/RAA.2019.097314

[128] A. Schafer, P. Ustohal, H. Harms, F. Stauffer, T. Dracos and A.J.B. Zehnder, Transport of bacteria in unsaturated porous media. *J. Contaminant Hydrol.* **33**, 149-169 (1998).
[129] G. Gargiulo, S. Bradford, J. Simunek, P. Ustohal, H. Vereecken and E. Klumpp, Bacteria transport and deposition under unsaturated conditions: The role of the matrix grain size and the bacteria surface protein. *J. Contaminant Hydrol.* **92**, 255-273 (2007).
[130] F. Huysman and W. Verstraete, Water-facilitated transport of bacteria in unsaturated soil columns - Influence of cell-surface hydrophobicity and soil properties. *Soil Biology Biochem.* **25**, 83-90 (1993).
[131] M.K. Kim, S.B. Kim and S.J. Park, Bacteria transport in an unsaturated porous media: Incorporation of air-water interface area model into transport modelling. *Hydrol. Processes* **22**, 2370-2376 (2008).
[132] T.K. Stevik, G. Ausland, J.F. Hanssen and P.D. Jenssen, The influence of physical and chemical factors on the transport of *E.coli* through biological filters for wastewater purification. *Water Res.* **33**, 3701-3706 (1999).
[133] G. Chen, J.L. Liu, K. Tawfiq, K. Yang and C. Banks, Colloid retention in unsaturated porous media as impacted by colloid size. *Particulate Sci. Technol.* **27**, 35-49 (2009).
[134] J.T. Crist, J.F. McCarthy, Y. Zevi, P. Baveye, J.A. Throop and T.S. Steenhuis, Pore-scale visualization of colloid transport and retention in partly saturated porous media. *Vadose Zone J.* **3**, 444-450 (2004).
[135] D.A. DiCarlo, Y. Zevi, A. Dathe, S. Giri, B. Gao and T.S. Steenhuis, In situ measurements of colloid transport and retention using synchrotron X-ray fluorescence. *Water Resources Res.* **42**, W12S05 (1-9) (2006).
[136] T.S. Steenhuis, A. Dathe, Y. Zevi, J.L. Smith, B. Gao, S.B. Shaw, D. DeAlwis, S. Amaro-Garcia, R. Fehrman, M.E. Cakmak and I.C. Toevs, Biocolloid retention in partially saturated soils. *Biologia* **61**, S229-S233 (2006).
[137] Y, Zevi, A. Dathe, B. Gao, B.K. Richards and T.S. Steenhuis, Quantifying colloid retention in partially saturated porous media. *Water Resources Res.* **42**, W12S03 (1-13) (2006).
[138] X.Q. Li, T.D. Scheibe and W.P. Johnson, Apparent decreases in colloid deposition rate coefficients with distance of transport under unfavorable deposition conditions: A general phenomenon. *Environmental Sci. Technol.* **38**, 5616-5625 (2004).
[139] S.A. Bradford and N. Toride, A stochastic model for colloid transport and deposition. *J. Environmental Quality* **36**, 1346-1356 (2007).
[140] N. Tufenkji, J. Redman and M. Elimelech, Interpreting biocolloid deposition patterns in packed-bed column experiments. *Abstracts Papers Amer. Chem. Soc.* **224**, U399-U399 (2002).
[141] N. Tufenkji, J.A. Redman and M. Elimelech, Interpreting deposition patterns of microbial particles in laboratory-scale column experiments. *Environmental Sci. Technol.* **37**, 616-623 (2003).
[142] Z. Li, R.F. Giese, W. Wu, M.F. Sheridan and C.J. van Oss, The surface thermodynamic properties of some volcanic ash colloids. *J. Dispersion Sci. Technol.* **18**, 223-241 (1997).
[143] B.A. Snyder, D.E. Aston and J.C. Berg, Particle-drop interactions examined with an atomic force microscope. *Langmuir* **13**, 590-593 (1997).
[144] U. Sindel and I. Zimmermann, Measurement of interaction forces between individual powder particles using an atomic force microscope. *Powder Technol.* **117**, 247-254 (2001).

DOI: 10.7569/RAA.2019.097314

[145] Y.K. Ma, Stochastic volatility effects on correlated log-normal random variables. *Adv. Mathematical Phys.* 7150203 (1-7) (2017).
[146] V.B. Fainerman and R. Miller, Dynamic surface tensions of surfactant mixtures at the water-air interface. *Colloids Surfaces A* **97**, 65-82 (1995).
[147] I.L. Povkh, R.V. Kucher, I.A. Shevchuk, A.I. Serdyuk, Z.M. Vashun and V.G. Lvov, Critical micelle concentrations of aqueous-solutions of a surfactant. *J. Appl. Chem. USSR* **51**, 1006-1009 (1978).
[148] J.R. Lu, E.A. Simister, R.K. Thomas and J. Penfold, Structure of the surface of a surfactant solution above the critical micelle concentration. *J. Phys. Chem.* **97**, 13907-13913 (1993).
[149] W.W. John, G.B. Bao, W.P. Johnson and T.B. Stauffer, Sorption of nonionic surfactant oligomers to sediment and PCE DNAPL: Effects on PCE distribution between water and sediment. *Environmental Sci. Technol.* **34**, 672-679 (2000).
[150] V.B. Fainerman, R. Miller, R. Wustneck and A.V. Makievski, Adsorption isotherm and surface tension equation for a surfactant with changing partial molar area. 1. Ideal surface layer. *J. Phys. Chem.* **100**, 7669-7675 (1996).
[151] G. Chen, Rhamnolipid biosurfactant behavior in solutions. *J. Biomater. Sci. Polymer Edition* **15**, 229-235 (2004).
[152] C.J. van Oss, Acid-base interfacial interactions in aqueous-media. *Colloids Surfaces A* **78**, 1-49 (1993).

DOI: 10.7569/RAA.2019.097314

